5-2020

Adaptation of a Low-Cost Hyperpolarization Technique for Use with Single-Sided NMR

Ruth A. Beaver

Adaptation of a Low-Cost Hyperpolarization Technique for Use with Single-Sided NMR

A thesis submitted in partial fulfillment of the requirement
for the degree of Bachelor of Science in Chemistry from
The College of William and Mary

by

Ruth A. Beaver

Accepted for **Honors**
(Honors, High Honors, Highest Honors)

Prof. Tyler K. Meldrum, Advisor

Prof. Christopher J. Abelt

Prof. David S. Armstrong

Prof. Kristin L. Wustholz

Williamsburg, VA
May 4, 2020

In this thesis, a low-cost hyperpolarization technique is adapted for use with single-sided nuclear magnetic resonance (NMR). Single-sided NMR suffers from inherent problems with low signal. This issue can be overcome using hyperpolarization, which allows for drastic enhancement of signal for the duration of a single measurement. Signal amplification by reversible exchange (SABRE) hyperpolarization was used due to its simplicity and cost effectiveness relative to other hyperpolarization techniques. While SABRE has been studied extensively on traditional NMR, it had not been adapted for single-sided NMR prior to this study.

A hyperpolarization apparatus was constructed to perform SABRE hyperpolarization in tandem with single-sided NMR. This apparatus was tuned and validated, then used to perform proof-of-concept ultrafast measurements. Ultrafast pulse sequences allow measurement of two different variables in a single measurement scan, allowing the most benefit from the single enhanced measurement scan from hyperpolarization. The initial results were promising, but further study will be necessary to address discrepancies between the hyperpolarized and control experiments.

Once further development of the technique has taken place, this new measurement setup has the potential to expand the measurement capabilities of single-sided NMR. The new system is able to perform single-scan ultrafast measurements, which allows for measurement of the evolution of two variables over short time spans. This capability combined with the open geometry of single-sided NMR could be useful for measurements of systems such as fuel cells, oil paints, biofilms, or time evolving interfaces, all of which are much more easily measured with single-sided NMR than traditional NMR.

Abstract

Nuclear magnetic resonance (NMR) suffers from inherent signal problems due to low levels of nuclear polarization at room temperature. These problems are especially prevalent in single-sided NMR, which allows for a more flexible measurement geometry and simpler, cheaper instrumentation than traditional NMR. Hyperpolarization techniques can remedy this by providing artificially high levels of polarization for a single measurement. Signal Amplification By Reversible Exchange (SABRE) hyperpolarization is particularly advantageous, since it can be produced quickly using relatively cheap and simple instrumentation. While SABRE hyperpolarization has been successfully demonstrated with traditional NMR, it has not yet been adapted for single-sided NMR. Here, an apparatus for performing SABRE hyperpolarization with single-sided NMR is constructed and verified. With this apparatus, signal enhancements of over two orders of magnitude are achieved. Finally, simple proof-of-concept measurements are performed to evaluate and demonstrate the potential of the new technique.

Acknowledgements

I would like to thank Mary Rooney for starting this project and creating the initial prototype of the hyperpolarization apparatus.

I would like to thank Dr. Molloy for his help in designing and constructing various aspects of the hyperpolarization apparatus and for his help in setting up measurements to verify the production of *para*-hydrogen production over the summer.

I would like to thank Will Henninger for constructing and helping to troubleshoot the custom lids for the bubbling apparatus as well as for his assistance in repairing a damaged catalyst coil.

I would like to thank Dr. Abelt for his help in setting up the traditional NMR measurements used for measurement of *para*-hydrogen production and high-field hyperpolarization.

I would like to thank Dr. Theis for his advice on setting up hyperpolarization measurements.

I would like to thank my fellow group members for creating a positive, fun lab environment. Special thanks to Madeline Brass and Justin Yu for mentoring me as a freshman, and to Elliot Kim, Jonathan Smailys, Mackenzie Kelley, John Cacciatore, and Caroline Thompson for their assistance in construction of the hyperpolarization apparatus and/or hyperpolarization measurements.

I would like to thank Dr. Pike for sending me down this research path as a freshman.

I would like to thank my family for their support of my academic ambitions and their tolerance of my enthusiasm for esoteric subjects.

Finally, I cannot thank ~~Dr. Meldrum~~ Tyler enough for making me the researcher I am today. Thank you for investing time and energy into a terrified, clueless freshman, for your unending patience with my unending mistakes, and most of all for your confidence in and support of me. This has truly been an amazing opportunity.

Contents

List of Figures

List of Tables

1 Introduction

Nuclear magnetic resonance (NMR) is a measurement technique which is able to probe the chemical environment around targeted nuclei through the interactions of those nuclei with magnetic fields. However, traditional measurement techniques require samples to fit in small glass tubes for measurement, limiting the types of samples which can be measured. Single-sided NMR, which has a more open geometry, extends the application of NMR techniques to larger or planar samples and allows measurements to be taken nondestructively. Unfortunately, the measurement geometry used for single-sided NMR also prevents it from replicating some of the most common measurement techniques used with traditional NMR. Instead, single-sided NMR is used for measurements of relaxation parameters (T_1, T_2) or diffusion coefficients (D). These variables can be used to deduce qualities such as the stiffness of a sample,[1] the degree of crosslinking in a polymer,[2] or the binding of different species in solution.[3] Single-sided NMR has been used successfully in many applications, including nondestructive measurements of paints,[1,4] food quality assurance,[5,6] oil well logging,[7] measurement of polymer curing,[2,8,9] and nondestructive, in-situ biological measurements.[10,11] However, single-sided NMR suffers from inherent problems with low signal. These problems are generally overcome by signal-averaging multiple measurements, which works well for many applications. However, this can result in long measurement times, which prevent the characterization of fast time-evolving samples, and may make measurements of extremely dilute samples prohibitively time-consuming.

Hyperpolarization techniques enable drastic enhancement of NMR signal for a single measurement by polarizing nuclei in the sample. Some of the most commonly used techniques are spin-exchange optical pumping (SEOP), dynamic nuclear polarization (DNP), and *para*-hydrogen polarization.[12] SEOP is one of the most effective techniques, and has been documented to produce polarizations as high as 90%[13] in ^{129}Xe. However, SEOP can only be used to directly polarize noble gas nuclei, which limits its applications.[12] DNP can also be a very effective technique, and has been documented to produce polarizations as high as 40%[13] in ^{13}C. It is more widely applicable than SEOP and can be used to target both carbon and hydrogen nuclei via interactions with radicals.

However, to get good results, SEOP requires expensive and bulky instrumentation, as well as liquid helium. While simpler DNP methods have been devised which can be performed at room temperature, the results are poor, on the order of less than 1% polarization in ^{1}H.[13]

Signal Amplification By Reversible Exchange (SABRE) hyperpolarization is a *para*-hydrogen polarization technique that can be performed with much more simple and inexpensive instrumentation than DNP or SEOP.[12] Despite its simplicity, it is fairly effective, with previously measured polarization of up to 11.5% in ^{1}H.[13] This combination of simplicity, low cost, and high performance makes it an attractive option for widely accessible hyperpolarization. While the use of SABRE hyperpolarization with traditional NMR has been studied extensively,[14] it has not yet been adapted for single-sided NMR. Since single-sided NMR in itself is a much simpler and less expensive instrumentation for performing NMR measurements, adapting SABRE hyperpolarization for single-sided NMR will enable wider application of hyperpolarization. SABRE hyperpolarization would be particularly useful in conjunction with ultrafast pulse sequences,[15] which utilize the magnetic field gradient present in single-sided NMR magnets to measure two different variables in a single measurement. However, ultrafast pulse sequences by themselves are somewhat limited due to the long measurement times required to resolve signal distributed over multiple measurement dimensions. Its use with SABRE hyperpolarization would speed up the measurements, so that one could take "snapshots" of the evolution of two variables over a short time span in a system. This capability combined with the open geometry of single-sided NMR could be useful for measurements of systems such as fuel cells, oil paints, biofilms, or time-evolving interfaces, all of which are much more easily measured with single-sided NMR than traditional NMR.

Here, SABRE hyperpolarization is demonstrated for the first time on single-sided NMR. An apparatus for SABRE hyperpolarization is constructed and tuned to maximize signal enhancement. This apparatus is then used in conjunction with an ultrafast D-T_2 pulse sequence to produce single shot measurements of multiple variables, which are compared to reference measurements. These measurements establish a novel technique which will expand the measurement capabilities single-sided NMR.

1.1 NMR Theory

Nuclear magnetic resonance uses the spins of atomic nuclei (typically protons) to probe chemical and physical properties of substances. Put simply, many atomic nuclei behave as though they are spinning. Since atomic nuclei are charged, the spinning behavior creates a magnetic dipole. When protons are placed in a magnetic field, they can either align with the field (low energy state) or align exactly opposite to the field (high energy state).* The distributions of nuclei aligned in each direction can be determined through the Boltzmann distribution, which relates the ratios of the populations of two energy states to the difference in energy between the two states and the temperature.

$$\frac{\#\text{ in high energy state}}{\#\text{ in low energy state}} = e^{-\frac{\Delta E}{k_B T}} \tag{1}$$

In this case, the difference in energy between aligning with or against the field is related to the strength of the magnetic field and the gyromagnetic ratio of the nuclei in question.

$$\Delta E = h\gamma B_0 \tag{2}$$

where γ, the gyromagnetic ratio, is used with units of Hz T^{-1}. In a magnetic field of typical strengths, the ratio of spins aligned with the field to those aligned against the field is very close to, but slightly less than one. This is problematic because the spins aligned with the field will cancel the signal generated by spins aligned against the field. This cancellation can be accounted for to determine a quantity called "polarization," which represents the percentage of spins in the sample that contribute to the measured signal.

*This is a useful simplification of what is actually happening. Nuclear spins are governed by the nuclear spin Hamiltonian $\hat{H} = -\gamma B_0 \hat{I}_z$, where γ is the gyromagnetic ratio of the nucleus, B_0 is the external magnetic field, and $\hat{I}_z$ is the spin angular momentum operator along the z axis (parallel to the magnetic field). Thus, the direction of the spin angular momentum for a nucleus that is not being measured cannot be known with certainty, only the probability of it pointing with or against the field, which correlates with the difference in energy between those states (γB_0). Furthermore, since the spin angular momentum operators for different axes are non-commuting operators, if the angular momentum is known along one axis it has no defined direction along the other axes, which complicates the explanation of spin precession about the z axis. However, the exact quantum mechanics of nuclear spin is beyond the scope of and not necessary for understanding this thesis.

The polarization is defined as:

$$p = \frac{N_\uparrow - N_\downarrow}{N_{total}} \tag{3}$$

which can be related to the field strength as:

$$p = \frac{1 - e^{-\frac{\Delta E}{k_B T}}}{1 + e^{-\frac{\Delta E}{k_B T}}} \tag{4}$$

In typical cases the polarization is very small. Consider a 400 MHz traditional NMR operating at room temperature: $k_B T = 4.115 \times 10^{-21} J$, and $\Delta E = 2.65 \times 10^{-25} J$, giving a polarization of about 0.003%, which corresponds to only about 30 protons per million protons in the sample contributing to the signal. The single-sided NMR used in this study, which operates at room temperature, provides a polarization of about 0.0001%, allowing only about 1 proton per million protons in the sample to contribute to the signal. The small polarization produced by NMR instruments is the cause of the signal to noise ratio (SNR) problems inherent to both traditional and single-sided NMR.

While the quantum mechanics of nuclear spin discussed above is necessary for an understanding of polarization, it becomes complicated when applied to NMR measurements. These measurements can be more easily understood using a simplified model where nuclear spins are treated as tiny, classical, magnetic dipoles. In this model, individual spins point in random directions due to thermal behavior; however, their interactions with the magnetic field create a tendency to partially align with the field. When all the contributions of all the spins are summed, there is a "bulk magnetization vector" aligning with the field.

When the bulk magnetization vector is "tipped" out of alignment with the external magnetic field, it will precess in a cone at the Larmor frequency (ω_0), which is given by:

$$\omega_0 = \gamma B_0 \tag{5}$$

where γ is the gyromagnetic ratio (42.577 MHz T^{-1} for ^{1}H) and B_0 is the external magnetic field strength. This precession is useful because it creates an oscillating magnetic field. Since a changing magnetic field induces an electric field, this can be detected as a current oscillating at the Larmor frequency. This current is typically very small, so to amplify the measurement a resonant circuit is used, which is tuned to the Larmor frequency.

In order to tip the bulk magnetization vector out of alignment, a radiofrequency (RF) pulse is used. This generates an oscillating magnetic field along an axis perpendicular to the direction of the external magnetic field. With an RF pulse of sufficient power, the frequency would not be important. However, in practical situations it is necessary to tune the frequency of the RF pulse to the Larmor frequency. As the bulk magnetization vector is tipped out of alignment with the external magnetic field, it will begin to precess. If the RF pulse is tuned to the Larmor frequency, it will "rotate" with the bulk magnetization vector and continue to tip the vector as it rotates. If the RF pulse is not tuned to the Larmor frequency it will be out of sync with the precession of the bulk magnetization vector and be unable to effectively tip the vector. The angle to which the bulk magnetization vector is tipped can be controlled by altering the time or power of the applied RF pulse.

Once the bulk magnetization vector is tipped out of alignment and begins to precess, it can be measured. The precession of the bulk magnetization vector creates a changing magnetic field, which can induce a current in a conductor. However, due to thermal effects, the bulk magnetization vector is very small and thus induces a very small current. In order to measure this current a resonant circuit tuned to the Larmor frequency is used, which will amplify signals close to its resonant frequency. The measured current can be resolved to correlate to the x and y components of the bulk magnetization vector over time. Since the z component of the bulk magnetization vector cannot be measured, a 90° tip angle will result in the largest measured signal. The measured signal for both the x and y components oscillates at the Larmor frequency due to the precession of the bulk magnetization vector. This signal exponentially decays with time, due to factors which will be addressed later.[16]

1.2 Single-Sided NMR

Traditionally, NMR is used to measure chemical shifts. Protons in different positions on a molecule experience slightly different magnetic fields due to interactions with other atoms on the molecule. Due to Equation 5, protons experiencing slightly different magnetic fields will have slightly different Larmor frequencies. The difference in Larmor frequency

between a proton on a molecule and a reference (typically tetramethylsilane) is known as the chemical shift, and can be used to deduce the structure of a molecule. However, to resolve chemical shifts it is necessary to have a highly homogeneous magnetic field. If the inhomogeneities in the external magnetic field are much larger than the magnetic field differences caused by molecular interactions, the differences in frequency due to differences in position in the external magnetic field will dominate and the chemical shifts will be impossible to resolve. The traditional NMR magnets able to resolve chemical shifts have highly homogeneous magnetic fields, generated by superconducting magnets submerged in liquid helium to provide enough magnetic field strength to provide good signal with few measurements. However, these magnets are limited by the available sample volume: measurements can only be taken of samples which can fit in a small tube with an inner diameter of about 3 mm.

Single-sided NMR involves an open geometry. A typical setup for single-sided NMR has a planar coil used for measurements situated on top of permanent magnets. This geometry allows for nondestructive measurements of large objects—for example, paintings—which cannot be done with traditional NMR. However, the open geometry of single-sided NMR also places limits on its measurement capabilities. The magnetic field created by the permanent magnets used in single-sided NMR is highly inhomogeneous (on the order of parts per thousand), making it impossible to use for measuring chemical shifts. Additionally, the permanent magnets create a magnetic field that is weak compared to the fields used in traditional NMR, which induces a smaller polarization in the sample, as demonstrated in Section 1.1, leading to smaller amounts of signal and longer measurement times. Since single-sided NMR cannot be used to measure chemical shifts, it is generally used to measure other parameters, such as relaxation times and diffusion coefficients.[16]

1.2.1 Spin-Lattice Relaxation (T_1)

One form of relaxation affecting NMR measurements is spin-lattice (T_1) relaxation. When a substance is exposed to an external magnetic field, it takes some time for the equilibrium magnetization (the state described by Equation 1) to occur. The z component of the bulk

magnetization vector (the component aligned with the field) is initially close to zero, but exponentially grows to its maximum value. This process can be described with the equation:

$$M_z(t) = M_{z,max}(1 - e^{-t/T_1}) \tag{6}$$

giving T_1, the spin-lattice relaxation time, which can be used as a measure of how fast spin-lattice relaxation occurs in a material. A smaller T_1 corresponds to a faster relaxation. The sample returns to 95% of its equilibrium magnetization after $3T_1$ and 99% after $5T_1$. T_1 reflects how effectively energy can be transferred from the spins to the surrounding material to allow decay back to equilibrium. This depends on the gyromagnetic ratio of the nuclei being measured; however, it is also affected by the ability of molecules and molecular segments to rotate. Typical T_1 times range from milliseconds to seconds.

Spin-lattice relaxation also describes the response of the bulk magnetization vector after it is tipped out of alignment with the external magnetic field. The bulk magnetization vector will exponentially re-align with the field, governed by the same T_1 time. Thus, it is important to know the T_1 of a sample when designing NMR experiments. If several experiments are being time-averaged to increase the signal to noise ratio, a delay of at least $3T_1$ must occur between measurements to allow the bulk magnetization vector to re-align. T_1 relaxation also places restrictions on SABRE hyperpolarization methods, which will be discussed later.[17]

1.2.2 Spin-Spin Relaxation (T_2)

Another process affecting decay of signal is spin-spin relaxation (T_2). T_2 relaxation describes loss of signal due to precessions of spins getting "out of sync," which cancels bulk magnetization in the x-y plane and thus causes a decay of measured signal. This phenomenon of spins getting "out of sync" is referred to as "dephasing". To measure T_2 on single-sided NMR, the Carr-Purcell-Meiboom-Gill (CPMG) pulse sequence is used.[18,19] A simple pulse experiment (tipping the bulk magnetization vector and watching the decay) cannot be performed on single-sided NMR. After the transmit/receive coil sends out an RF pulse, the residual current in the coil must decay to zero before the receiver amplifier is switched on, otherwise the receiver could be damaged. However, in single-sided NMR,

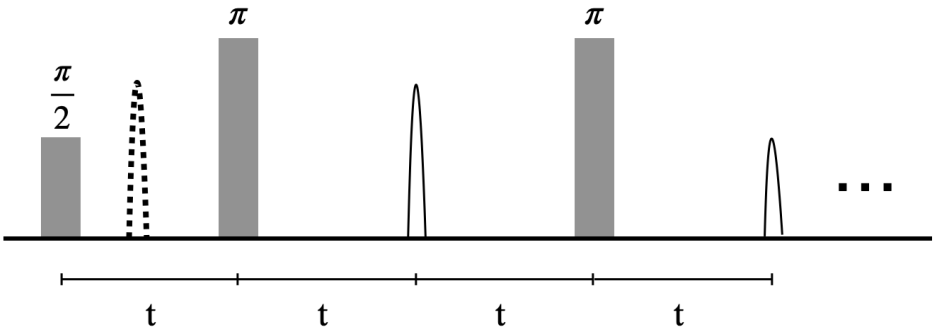

Figure 1: The CPMG pulse sequence used for measuring T_2 relaxation.

the time it takes for the current to decay is much longer than the time it takes for the signal to decay, due to the inhomogeneity of the magnetic field used. This means that the measurable signal will have decayed to zero by the time it is safe to turn on the receiver amplifier and take a measurement.

To get around this, the CPMG pulse sequence (Figure 1) generates "echoes" of the original signal which can be detected after a delay, allowing time for the current to decay before measurements. The CPMG starts with a 90° pulse to start the precession of the bulk magnetization vector. Initially, this causes spins in the sample to precess together. However, due to field inhomogeneities and differing chemical environments not all the spins experience the same magnetic field, which causes them to precess at different frequencies (Equation 5). Since nuclei in the sample are precessing at slightly different frequencies, as time goes on they will dephase and begin to cancel each other out, leading to a decay of signal.

This can be reversed if a 180° pulse is applied to the sample, after a delay. During the initial delay, spins precessing faster will travel a larger distance, and spins precessing slower will travel a smaller distance. After inversion, the relative positions of the spins in the x-y plane "flip," but they continue precessing in the same direction at the same frequency. This leads to an "echo" of signal, where the faster spins catch up to the slower spins and re-align, allowing signal to be measured. The time at which this echo occurs is determined by the delay between the 90° and 180° pulses. Additional 180° pulses can be applied (after appropriate time delays) to generate additional echoes.

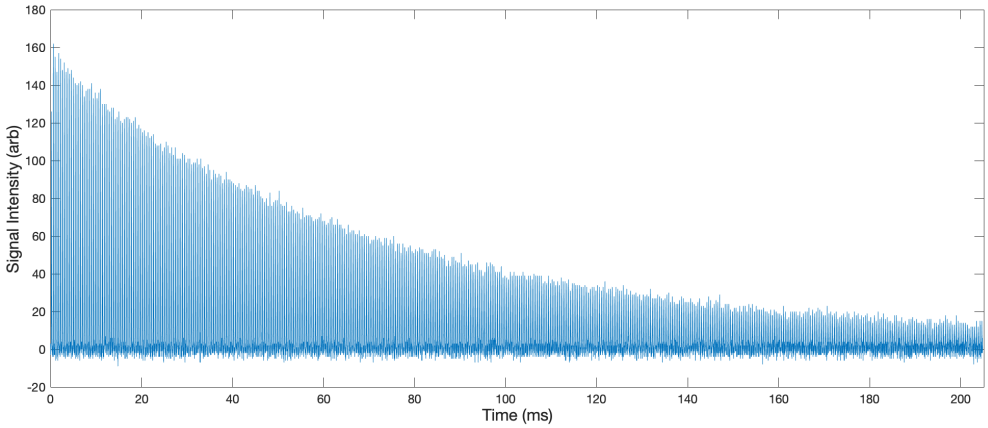

Figure 2: An example CPMG dataset. Echoes produced by the pulse sequence decay exponentially and can be fitted to an exponential curve to yield T_2.

However, the signal produced by progressive echoes decays exponentially. This is mostly caused by dipolar interactions between nearby spins. Nuclear spins precessing in close proximity with each other will experience time-dependent forces as the components of their magnetic dipoles in the x-y plane align and anti-align with each other. This causes interruptions to the spin precession frequencies. The CPMG echoes depend on spin precession frequencies staying constant, so when interruptions to the precession frequency occur, spins no longer line up exactly during an echo, which reduces the measured signal. This effect increases with time, leading to an exponential decay of echo signal with repeated echoes (see Figure 2). This decay can be fitted to an exponential function of the form $f(t) = Ae^{-t/T_2} + C$, where A and C are the scaling term and offset correction, to give the T_2 relaxation constant. When spins are allowed to move freely through the sample, interactions between spins tend to average out, leading to slower decay of signal and a larger T_2. When spins in a sample are held near each other, for example, in a rigid polymer matrix, these interactions have a more pronounced effect, leading to a faster decay of signal and a smaller T_2.

1.2.3 Self-diffusion Coefficient (D)

Another variable that can be measured with single-sided NMR is a substance's self-diffusion coefficient (D), a quantity typically measured in units of $\mathrm{m}^2\ \mathrm{s}^{-1}$ which represents the speed with which a molecule of a substance is able to diffuse through that substance.

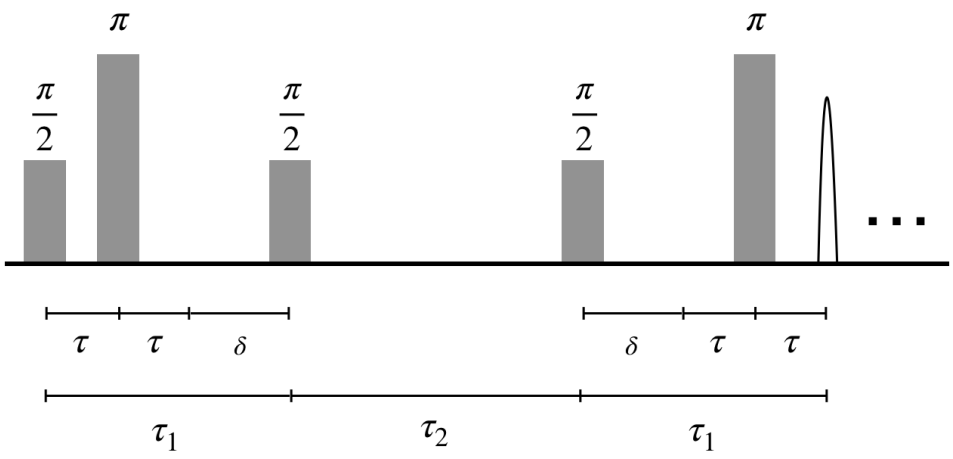

Figure 3: The pulse sequence used to measure the self-diffusion coefficient. Initially, a 90° pulse is applied to the sample, which causes the spins to begin to precess and dephase in the x-y plane. After a time τ, a 180° pulse is applied, which flips the spins and causes them to rephase at a time τ after the pulse. The spins are then allowed to dephase for a time δ, after which a 90° pulse is applied, which flips the spins to point along the z axis, encoding their current phase. After a time τ_2, a 90° pulse is applied to the sample, which brings the spins back into the x-y plane where they begin to rephase, since the two successive 90° pulses have a similar effect to a single 180° refocusing pulse. The spins are maximally rephased after a time δ, and are then allowed to dephase for a time τ. Then a 180° pulse is applied to the sample, resulting in rephasing of spins to create a stimulated echo which can be measured. This is typically followed by a series of 180° pulses to acquire additional echoes, similarly to a CPMG.

The self-diffusion coefficient decreases with increasing viscosity and decreasing temperature. Diffusion can be measured with NMR techniques when a magnetic field gradient is present. As a spin diffuses along the magnetic field gradient, its precession frequency will change (Equation 5), which prevents full refocusing from happening during echo acquisition. This causes irreversible signal loss, which can be measured to determine the average distance molecules have moved along the gradient. Single-sided NMR is particularly well-suited for measuring diffusion coefficients because of the inherent field gradient present in the measurement setup.

Signal loss from diffusion effects is typically a smaller factor than signal loss from T_2 relaxation, and thus will not interfere with most CPMG measurements. In order to measure diffusion, a different pulse sequence is used, which is pictured in Figure 3. This pulse sequence extends the experiment longer than a CPMG sequence would allow, allowing molecules to diffuse further during the experiment, enhancing the effect of diffusion.

Signal loss due to diffusion is isolated from signal loss due to relaxation by restricting measurement parameters. T_2 relaxation only occurs during the two τ_1 periods, since these are the only times where the bulk magnetization vector has x-y components.* T_1 relaxation occurs throughout the entire experiment, but since the experiment is designed so that $\tau_2 \gg \tau_1$, the effects of T_1 relaxation during the τ_1 period are negligible compared to its effects during the τ_2 period. Thus, T_1 relaxation effectively only occurs during the τ_2 period. To isolate relaxation effects from diffusion effects, τ_1 and τ_2 are held constant. This holds signal loss due to relaxation effects constant between measurements. Diffusion is probed by varying δ, which allows different amounts of time for changes in Larmor frequency due to diffusion during the τ_2 period to cause signal loss.†

D is determined by comparing the signal amplitude of the stimulated (initial) echo between measurements. Signal attenuation can be expressed as a product of signal attenuation due to all factors currently acting on the system:

$$A_{tot} = A_D A_{T_1} A_{T_2} \tag{7}$$

Where attenuation is a number greater than 0 but less than or equal to 1, with 1 corresponding to no attenuation of signal. The attenuation due to T_1 and T_2 relaxation can be expressed simply as exponentials with the relevant times where relaxation was allowed to occur:

$$A_{T_1} = e^{-\tau_2/T_1} \quad \text{and} \quad A_{T_2} = e^{-2\tau_1/T_2} \tag{8}$$

In the case of isotropic diffusion through a constant field gradient the attenuation due to diffusion can be expressed as:

$$A_D = e^{-b(\delta)D} \tag{9}$$

where $b(\delta)$ is a constant depending on the experimental parameters, which, in the case of isotropic diffusion through a constant field gradient is defined as:

$$b(\delta) = \gamma^2 G^2 [\tau_1^2 - 3\tau_1^2\delta + 3(\tau_1 + 2\tau_2)\delta^2 + 3\delta^3] \tag{10}$$

*Some magnetization remains in the x-y plane after the second 90° pulse, but this can be regarded as lost signal as it does not show up in the measured echoes.

†In order to vary δ without varying τ_1 or τ_2, τ must be varied in tandem with δ.

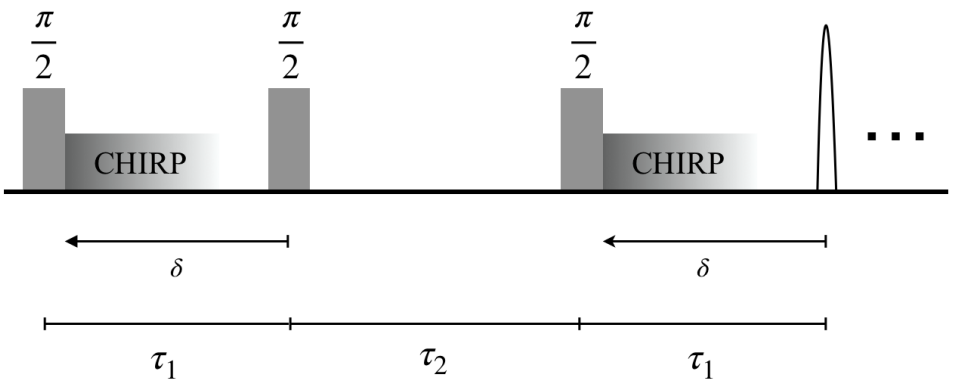

Figure 4: The pulse sequence used to perform ultrafast D-T_2 measurements. The 180° pulses used in the traditional diffusion experiment are replaced with frequency-sweeping CHIRP pulses, which perform 180° flips of different slices of the sample at different times, allowing multiple values of δ to be tested in a single experiment. This is followed by a series of 90° pulses (as in a CPMG) to measure T_2.

where $G = \frac{dB}{dz}$ is the magnetic field gradient. Thus, the overall attenuation of signal during a diffusion experiment (in the case of isotropic diffusion through a constant field gradient) can be expressed as:

$$A_{tot}(\delta) = e^{-b(\delta)D} e^{-\tau_2/T_1} e^{-2\tau_1/T_2} \tag{11}$$

Importantly, since τ_1 and τ_2 are held constant, the only dependence on δ is in the expression for diffusion attenuation. Thus, changes in measured signal due to changes in δ can be used to calculate D.

During diffusion measurements, it is also possible to measure the T_2 of the substance by adding additional echoes after the stimulated echo (similar to the CPMG sequence) and measuring the exponential decay of signal through these echoes. This is convenient to do because acquiring additional echoes is typically very fast compared to the total measurement time.

1.2.4 Ultrafast D-T_2

Traditional diffusion experiments are time-consuming, since they involve multiple experiments, each of which must be repeated if signal averaging is necessary. The ultrafast D-T_2 pulse sequence (pictured in Figure 4) allows probing of diffusion through a single experiment. Ultrafast D-T_2 was adapted to single-sided NMR in 2018 by King et. al.,[15] and

is based on similar principles to traditional diffusion measurements. Instead of varying the time of 180° pulses between experiments, frequency-sweeping CHIRP pulses are used. As shown in Equation 5, the Larmor frequency of a nuclei depends on the magnetic field it experiences. In a single-sided NMR experiment, a constant field gradient is present,* thus, the precession frequency of nuclei in the sample varies continuously with position along the field gradient. A frequency-sweeping CHIRP pulse linearly varies its frequency over time, and thus targets different positions at different times. This has the effect of varying δ with position along the field gradient. To find attenuation of signal as a function of δ, the signal is measured as a function of position along the field gradient using a Fourier transform of each echo. This can be used to determine the diffusion coefficient. T_2 is measured by following the pulse sequences with a series of 180° pulses to read echoes (as is done in a CPMG pulse sequence) and the signal decay through progressive echoes is found. An inverse Laplace transformation of the data can be used to produce a plot correlating D and T_2 of various components within a sample.

1.3 SABRE Hyperpolarization

Due to the low strength of the magnetic fields used, single-sided NMR has low signal. As shown in Equation 1, the polarization decreases as magnetic field strength decreases. As discussed, this is a major problem because measured signal is proportional to the polarization of the sample. One way to get around this issue is to average measurements over many samples, removing noise. While this strategy works for many applications, it can make measurements of thin or dilute samples impractically long, since SNR scales with the square-root of the number of measurements averaged. Samples giving very small signal can require thousands of measurements to resolve the signal, which may take up to several hours, depending on the measurement parameters being used and the T_1 of the sample. Furthermore, this technique can make it difficult to measure time-dependent phenomena on short time scales.

*While magnetic fields don't fall away linearly, they can be approximated as linear within a small enough area. The sensitive region of the single-sided NMR used in these experiments has a length 300 μm along the direction of the field gradient, which allows this approximation to be made.

Hyperpolarization fixes the problem of low signal by taking spins anti-aligned with the field and flipping them to alignment with the field, thus increasing the spin polarization beyond the thermal (Boltzmann) distribution. This has a drastic impact on signal, since it is both removing cancellation of spins and adding more spins aligned in a direction that produces signal. However, hyperpolarization signal enhancement only lasts for the duration of a single measurement scan: the process of measuring causes the polarization to return to thermal equilibrium.*

SABRE hyperpolarization achieves this by transferring spin polarization from *para*-hydrogen to the substrate. This is done by dissolving both the substrate and the SABRE catalyst in a deuterated solvent, allowing the substrate to coordinate to the catalyst. *Para*-hydrogen enriched gas is bubbled into the solution at elevated pressures, which dissolves it into the solution so it can coordinate with the catalyst. This bubbling is done at a specific magnetic field strength which promotes polarization transfer. As the substrate and *para*-hydrogen coordinate to and dissociate from the catalyst, hyperpolarization of the substrate is produced. This bubbling is done until sufficient hyperpolarization is built up, at which time the sample is transferred to a magnet for measurement.

In general, for successful SABRE hyperpolarization to occur, the substrate of interest must be able to coordinate reversibly to the SABRE catalyst.† This tends to promote substances with multiple bonds to nitrogen as hyperpolarization substrates.[20] Furthermore, for optimum performance the exchange rate at the catalyst needs to be tuned for different substances to account for different optimum coordination times at the SABRE catalyst.[21] This can be done by altering the composition of ligands on the SABRE catalyst. The most common hyperpolarization substrate for proof-of-concept studies is pyridine, which is well-known to behave optimally with the IrCl(COD)(IMes)‡ catalyst.[22]

*This occurs because in nearly all measurement techniques full T_1 relaxation of the sample occurs between measurement scans to "reset" the sample, which returns the sample to thermal equilibrium.

†Schemes have been developed which allow hyperpolarization of substrates which do not coordinate with the catalyst through interactions with a substance which can coordinate to the catalyst. These will be discussed later.

‡Where COD = cis,cis-1,5-cyclooctadiene and IMes = 1,3-bis(2,4,6-triethyl-phenyl) imidazol-2-ylidene

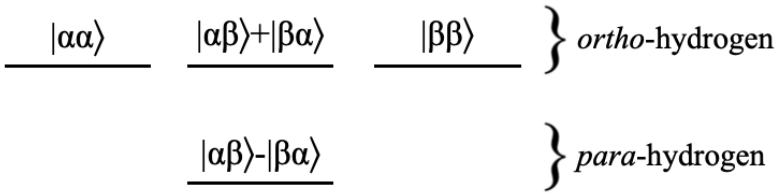

Figure 5: A simplified energy level diagram of the spin states of molecular hydrogen. Here α corresponds to spin "up" and β corresponds to spin "down" for one of the nuclei in molecular hydrogen.

1.3.1 *para*-Hydrogen

In order to perform SABRE hyperpolarization, a specific nuclear spin state of hydrogen called *para*-hydrogen must be used. Molecular hydrogen can be in one of four possible spin states (pictured in Figure 5). Three of these spins states correspond to symmetric, triplet states. These three states are degenerate, and known as *ortho*-hydrogen. The fourth state is an asymmetric, singlet state which has a lower energy, and is known as *para*-hydrogen. This state is useful for hyperpolarization because of its rigidly defined asymmetry, and can be easily isolated due to its energy difference with *ortho*-hydrogen states.

Since at room temperature there is sufficient energy to populate all four nuclear spin states essentially equally, the fraction of *para*-hydrogen in room temperature hydrogen gas at thermal equilibrium is about 25%. SABRE hyperpolarization requires hydrogen gas that is enriched with *para*-hydrogen beyond thermal levels, and is more effective with higher levels of *para*-hydrogen enrichment. At 77 K (the boiling point of liquid nitrogen) the fraction of *para*-hydrogen at equilibrium is about 52%, and at 20 K hydrogen is nearly 100% *para*-hydrogen.[21] However, the conversion between *ortho*- and *para*-hydrogen is slow (on the order of weeks). Generally, a paramagnetic catalyst (such as iron oxide hydroxide, FeO(OH)) is used to speed up the conversion. Conveniently, once the gas is converted, the conversion back to thermal equilibrium at room temperature is slow and can be ignored.[21]

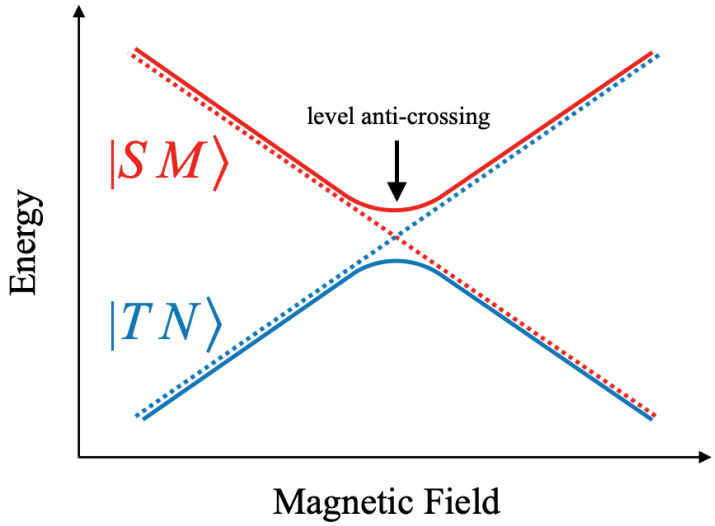

Figure 6: Simplified diagram of level anti-crossing between the states $|SM\rangle$ and $|TN\rangle$. At the magnetic field where the LAC occurs, the two energy states would be degenerate, but they interact to prevent the degeneracy from occurring. This results in interactions between the two states and a minimum in the energy differences of the states.

1.3.2 Polarization Transfer

Once *para*-hydrogen and the substrate bind to the catalyst, the spins of the *para*-hydrogen nuclei and the hydrogen nuclei of the substrate interact through J-coupling. J-coupling occurs when spins are close enough to each other in space to influence the energy of each others' spin states. This results in coupled spin states, since the energy of one spin's state depends on the state of the other spin. The J-coupling "frequency" refers to the magnitude of the spin state energy shift due to J-coupling interactions. The energy state of the SABRE catalyst system can be described as $|AB\rangle$, where A describes the state of the two hydrogen nuclei coordinated to the catalyst and B describes the polarization of a substrate molecule coordinated to the catalyst. The hydrogen nuclei can exist in the singlet state S (corresponding to *para*-hydrogen) or in one of three degenerate triplet states T (corresponding to *ortho*-hydrogen). The polarization of the substrate will simply be described as a state M or a state N, involving select chemically equivalent nuclei on the substrate. There exists a level anti-crossing (LAC) between the states $|SM\rangle$ and $|TN\rangle$, where the two states interact to prevent degeneracy (see Figure 6). The system can be placed at the LAC by tuning the external magnetic field such that the energy difference

between states $|SM\rangle$ and $|TN\rangle$ due to the external magnetic field is equal to the energy difference caused by J-coupling between the substrate and *para*-hydrogen nuclei. When the system is at or near the LAC, the energy difference between states $|SM\rangle$ and $|TN\rangle$ is at a minimum, which is advantageous to transfer between the two states. Furthermore, at the LAC, the eigenstate of the system is a combination between $|SM\rangle$ and $|TN\rangle$, which promotes transfer between the two states.[23] Strong coupling between the substrate and *para*-hydrogen nuclei will induce transitions between the higher energy state $|SM\rangle$ and the lower energy state $|TM\rangle$ when the system is at or near the LAC. The system as a whole will evolve towards a thermal equilibrium where the lower energy state has a larger population than the higher energy state.[21,23,24]

The transition from state $|SM\rangle$ to state $|TN\rangle$ results in conversion of the substrate from the M state to the N state selectively, thus enriching the N state beyond thermal levels. When other spin state combinations bind to the catalyst (for example, perhaps the state $|TM\rangle$ forms), there is no LAC to induce a transition and thus the spin states are unaltered. Some time after coordination, hydrogen and substrate will dissociate from the complex and allow new *para*-hydrogen and substrate molecules to interact. This time varies from about 33 ms to 1s depending on the ligand on the SABRE catalyst, which can be altered to fine-tune the exchange rate to optimum levels for the substrate.[21] This reversible exchange results in a build-up of polarization in the sample. However, decay due to T_1 relaxation limits this polarization build-up, as the hyperpolarized spins will slowly decay back to thermal equilibrium. Thus, polarization in the sample will increase and approach a limit set by the T_1 of the substrate, as well as other experimental parameters such as the *para*-hydrogen enrichment and the exchange rate of the catalyst. Once the sample is removed from the polarization field and bubbling of *para*-hydrogen stops, the hyperpolarization of the sample will decay exponentially to thermal equilibrium through T_1 relaxation, since no new polarization is being formed. Thus, quick measurement of a hyperpolarized sample is essential to prevent signal loss.

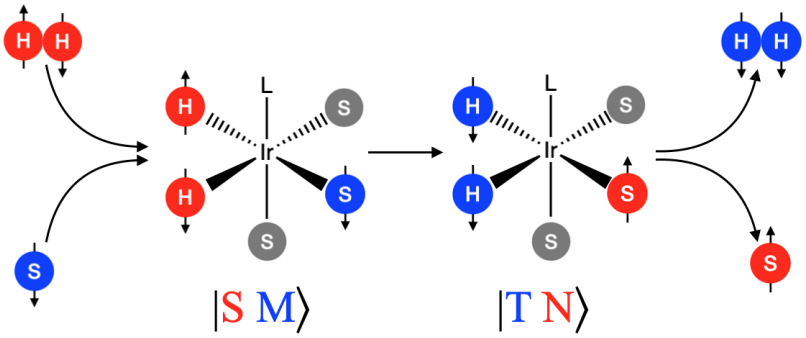

Figure 7: A diagram illustrating the polarization transfer process. Here, circles labeled "H" are hydrogen atoms and circles labeled "S" are substrate molecules. Gray substrate molecules are substrate molecules which are coordinated to the complex but do not participate in hyperpolarization. Initially, *para*-hydrogen and substrate coordinate to the SABRE catalyst. Polarization is transferred from *para*-hydrogen to the substrate, converting the *para*-hydrogen to *ortho*-hydrogen and changing the spin state of the substrate.

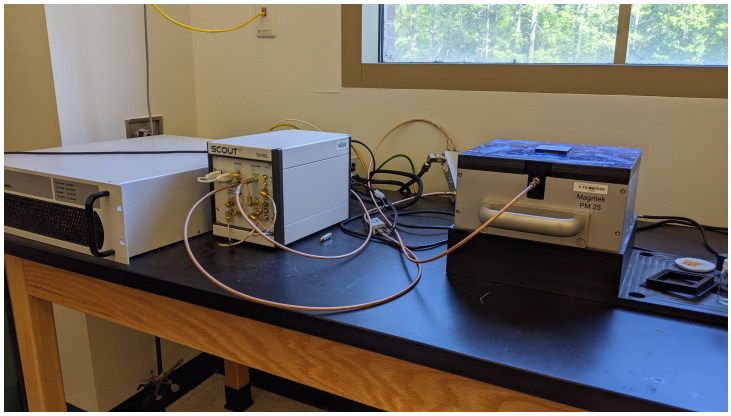

Figure 8: The single-sided magnet and spectrometer used to acquire single-sided NMR measurements.

2 Methodology

2.1 Instrumentation

2.1.1 NMR

Single-sided NMR measurements were taken with a PM25 NMR-MOUSE (Magritek; Wellington, New Zealand) with a Scout spectrometer (Tecmag; Houston TX). This system is pictured in Figure 8. The PM25 has a magnetic field of approximately 0.3 T, a field gradient of 6.59 T/m, and a proton frequency of 13 MHz. During measurements, 20 mm spacers were used, which positioned the transmit/receive coil within 5 mm of the sensitive

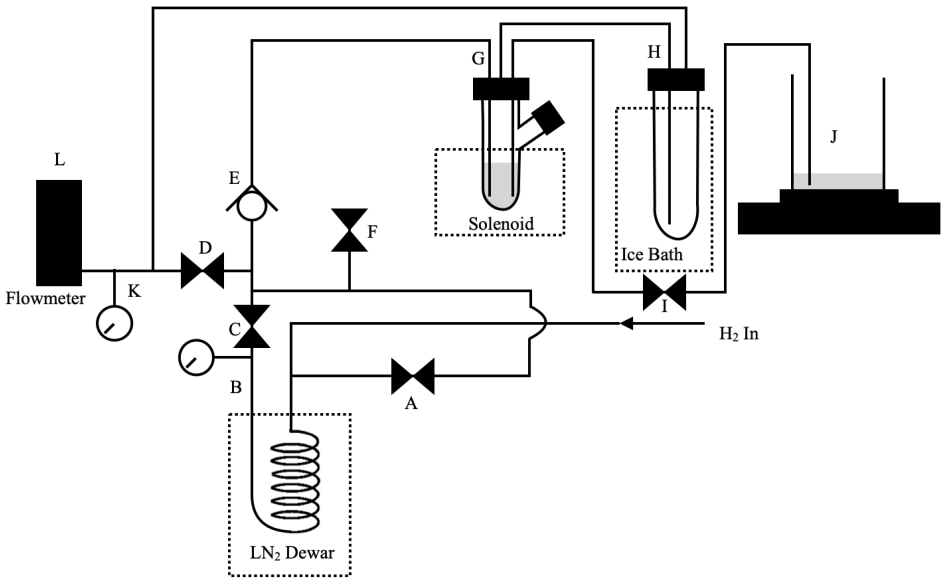

Figure 9: A schematic of the hyperpolarization apparatus used.

region. Glass microscope slides were placed on top of the magnet to elevate sample vials so that the sensitive region was within the liquid sample.

Traditional NMR measurements used to verify *para*-hydrogen production and to initially test the hyperpolarization apparatus were produced on a Varian Mercury VX-400 NMR with a reference frequency of 400.181 MHz.

2.1.2 Hyperpolarization Apparatus

A gas manifold for performing SABRE hyperpolarization for use with single-sided NMR was developed and validated. In general, this manifold allows hydrogen gas to pass over a liquid-nitrogen-cooled catalytic bed (for enrichment of *para*-hydrogen), then into a sample chamber for polarization transfer. A schematic of the final apparatus is shown in Figure 9. When valves A and F are closed and valve C is open, gas flows through a double-wrapped copper tubing coil (Hi Proof Products) submerged in liquid nitrogen. This cools the gas to near 77 K before it passes over the conversion catalyst (Iron Oxide Hydroxide, FeO(OH)), which is contained in the straight section of tubing running from the bottom of the copper coil out of the dewar. This catalyzes the equilibration of hydrogen gas spin states, leading to enrichment with *para*-hydrogen due to the low temperatures. Enough catalyst was used to fill a 25 cm length of tubing. The catalyst was held in place with

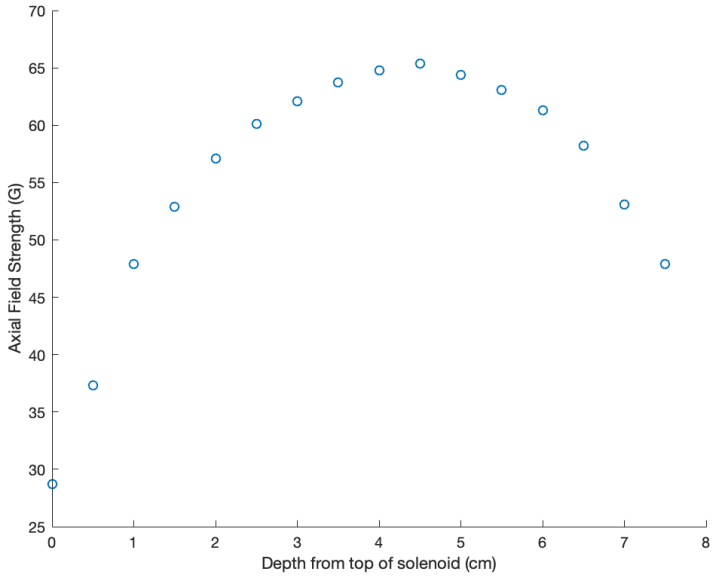

Figure 10: Measurements of the axial field strength along the depth of the handmade solenoid used to produce the J-coupling field.

glass wool plugs on either side. The catalyst was baked in a vacuum oven for 24 hours before use to drive off residual water.

After passing through the liquid nitrogen dewar, if valve D is closed and valve C is open, gas is bubbled through a solution containing the SABRE catalyst and substrate (G in Figure 9). A check valve (IDEX) is used to prevent backflow of solution into the gas manifold due to pressure differences (E in Figure 9). The gas is bubbled through the SABRE solution at a pressure of 50 psi. Pressure is monitored using pressure gauges B and K (McMaster-Carr), which allow monitoring of pressure going into the bubbling setup and coming out of the bubbling setup, respectively. The pressure vessel used for bubbling was obtained from Ace Glassware, and custom lids were manufactured which allow pressure-tight connections with teflon tubing. As gas is bubbled through the solution, it leaves through teflon tubing sealed to the lid and passes through another pressure vessel (H in Figure 9) which is submerged in an ice bath. This condenses volatile solvent that may have evaporated from the SABRE solution during bubbling, protecting the gas manifold and allowing for recycling of evaporated solvent. Gas leaves the second pressure vessel and is returned to the gas manifold, where the pressure is monitored and the flow rate is controlled with a variable flowmeter (McMaster-Carr).

The bubbling pressure vessel rests inside a solenoid, which produces a magnetic field of approximately 65 G in the volume where the SABRE solution is present. The solenoid consists of a 3D-printed mount, hand wound with solenoid wire. The field produced by the solenoid along its axis was measured using a handheld gaussmeter (see Figure 10). This revealed that the magnetic field strength falls away near the edges of the solenoid, and thus the strength is not uniform within the solenoid. A rubber plug approximately two centimeters in height was used to elevate the bubbling vessel so that the solution would rest in the center of the solenoid where the magnetic field strength was most uniform, allowing for close matching of the J-coupling field over the entire volume of sample. The solenoid was positioned near the NMR magnet in a dead zone where the magnetic field is approximately zero. This is the closest it can get to the magnet without the magnet's field interfering with polarization transfer, and is thus the best position for the solenoid to minimize transfer time.

Solution is transported to an open beaker on top of the single-sided magnet (J in Figure 9) for measurements by using the pressure differential between the pressure vessel and the open beaker. When gas is bubbling through the solution, if the valve at I in Figure 9 is opened, the pressure in the bubbling vessel will drive solution out of the pressure vessel and into the beaker. The teflon tubing running from the bubbling vessel to the beaker is kept as short as possible to minimize transport time. After a measurement takes place, the solution is removed from the beaker and pipetted back into the pressure vessel (after pressure has been released by closing valve C and waiting for gas to vent from the flowmeter) through the side opening.

2.1.3 Validation of *para*-hydrogen Production

The initial prototype of the hyperpolarization apparatus was not functional. As a part of troubleshooting this issue, it was necessary to determine whether the catalyst coil was actually producing *para*-hydrogen. A high-field NMR test was devised to detect *para*-hydrogen enrichment. Since *para*-hydrogen is the singlet state of hydrogen, it does not produce NMR signal. All NMR signal from hydrogen gas comes from *ortho*-hydrogen, the triplet state. At room temperature, equilibrium hydrogen gas is 25% *para*-hydrogen

enriched, at 77 K equilibrium hydrogen gas is 52% *para*-hydrogen enriched. Thus, the predicted level of *para*-hydrogen enrichment should be detectable as a decrease in measured NMR signal by roughly a factor of 3.

Hydrogen gas was dissolved in acetone (doped with a small amount of deuterated acetone to facilitate locking) by pressurizing a Norell valved NMR tube to 50 psi and inverting several times. Acetone was chosen as the solvent due to the good solubility of hydrogen gas in acetone and the separation of acetone NMR peaks from the expected location of dissolved hydrogen gas peaks.[25] Since the solvent used (acetone) produced much more NMR signal than the small concentration of dissolved hydrogen gas, a solvent saturation technique was used to suppress the solvent peaks. The dissolved hydrogen peak was located and verified through comparison of measurements at increasing pressures of hydrogen gas. The identified peak was at a chemical shift of 4.55 ppm, matching literature observations.[26] Duplicate samples of room temperature hydrogen gas and cold hydrogen gas were measured alternately, with fresh solution for each measurement. Room temperature hydrogen gas could be produced from the manifold even when the catalyst coil was submerged in liquid nitrogen by closing valve C and opening valve A (see Figure 9).

Initially, the difference between signal produced by room temperature and cold hydrogen gas were not enough to support that the expected degree of *para*-hydrogen production was occurring (see Figure 11 and Table 1). There was a small difference between room temperature and cold hydrogen gas signal, suggesting *para*-hydrogen enrichment may have been occurring to a smaller extent. Alterations were made to the original catalyst coil, which consisted solely of a double-wound coil of copper tubing with the catalyst inside. Additional straight tubing packed with catalyst along a length of 25 cm was added after the coil. Measurements of gas produced with this coil showed the expected signal decrease (see Figure 11 and Table 1). The increase in *para*-hydrogen enrichment after alterations may have been caused by the longer cooling path before gas reached the catalyst, or it may have been caused by an increase in the amount or packing density of catalyst used.

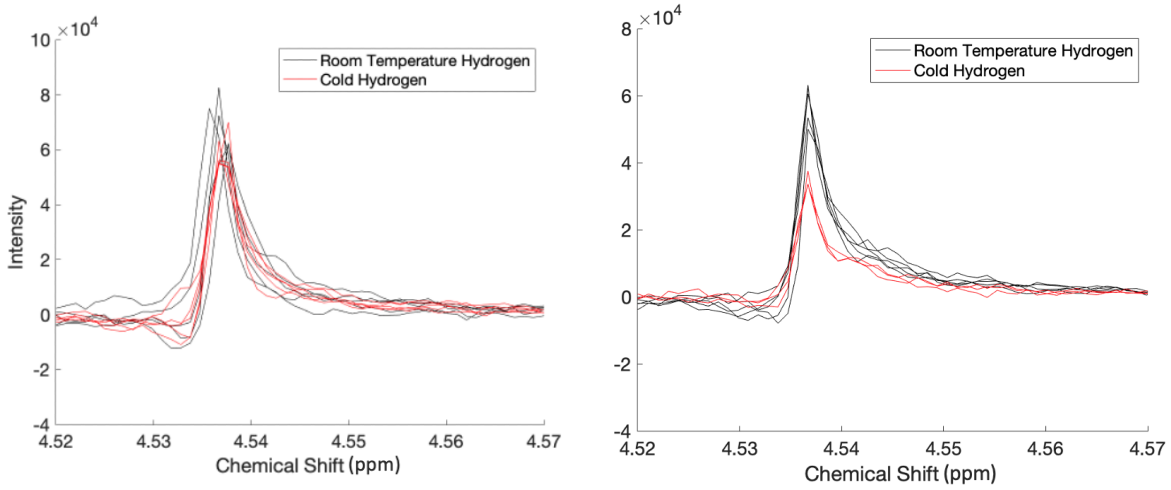

Figure 11: Comparison of measured *para*-hydrogen enrichment production produced by the original catalyst coil (left) and the altered catalyst coil (right).

	Original Catalyst Coil	**Altered Catalyst Coil**
Room Temperature Hydrogen Signal Intensity	390 ± 30	320 ± 40
Cold Hydrogen Signal Intensity	340 ± 40	216 ± 7
Ratio of Cold:Room Temp. Signal Intensity	0.9 ± 0.1	0.7 ± 0.1

Table 1: Comparison of integrated signal intensities of gas produced by the original catalyst coil and the altered catalyst coil. Uncertainties are derived from standard deviation in the dataset. Units of signal intensity on NMR are arbitrary.

2.2 Hyperpolarization Procedures

Initial testing of hyperpolarization was done at high-field, with polarization transfer occurring in the fringe field of the magnet at a location identified with a gaussmeter to have a magnetic field of approximately 65 G. For these experiments, a solution containing 2 mM of SABRE catalyst* (University of York Center for Hyperpolarization in Magnetic Resonance; York, England) and 50 mM pyridine (Sigma-Aldrich) in deuterated methanol (Sigma-Alrich) was used, at the advice of Dr. Thomas Theis at NC State. For these measurements, solution in a valved NMR tube was pressurized to 50 psi with *para*-hydrogen enriched gas, then inverted several times in the 65 G region of the fringe field, then immediately transferred to the magnet for measurement. The same solution was used for successive measurements, and the NMR tube was vented and repressurized between measurements. Initial measurements showed no signal enhancement, as the catalyst was still in the process of being activated. Later measurements showed modest signal enhancement, validating the hyperpolarization apparatus (see Figure 12).

Hyperpolarization on low-field NMR was done with a solution containing 18 mM of SABRE catalyst and 450 mM of pyridine. The concentration was increased relative to the high-field experiments to compensate for the insensitivity of single-sided NMR. 18 mM represents the approximate solubility limit of the catalyst in methanol, and the pyridine concentration was increased so that the catalyst to pyridine ratio (1:25 by mass) remained the same. In the finalized hyperpolarization setup, the hyperpolarization solution was mixed and bubbled with room temperature hydrogen for half an hour at a pressure of 50 psi to activate the SABRE catalyst. Then, the catalyst coil was submerged in liquid nitrogen to begin producing *para*-hydrogen enriched gas. Before each measurement, the hyperpolarization solution was bubbled with *para*-hydrogen enriched gas for 30 seconds while in a field of approximately 65 G produced by the solenoid. To take a measurement, valve I (labeled on Figure 9) was opened, allowing solvent to dispense into an open container on the magnet. The valve was closed after an adequate amount of solution was dispensed (about 1 mL). Sample transport was able to be achieved in

*IrCl(COD)(IMes), where COD = cis,cis-1,5-cyclooctadiene and IMes = 1,3-bis(2,4,6-triethyl-phenyl) imidazol-2-ylidene

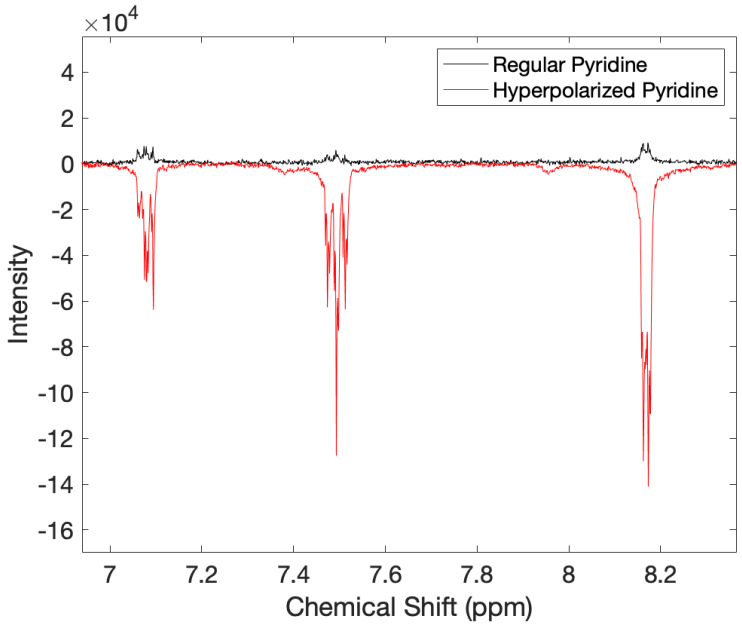

Figure 12: Hyperpolarization measured using high-field NMR to validate the hyperpolarization apparatus. A spectrum of the solution without hyperpolarization is shown in black and the hyperpolarized spectrum is shown in red. The hyperpolarized signal has negative intensity because SABRE hyperpolarization populates the higher energy spin state more than the lower energy spin state, the reverse of thermal behavior. An overall enhancement of $\epsilon = 10$ was achieved (determined from dividing the integral of the hyperpolarized peaks by the integral of the regular peaks). This corresponds to a polarization of 0.03%. (Methods used to calculate polarization are discussed in Section 2.3.)

under 2 seconds, which was important to minimize T_1-related signal loss, as discussed previously. Immediately after the sample was dispensed, an NMR measurement was started. An attempt was made to standardize the time for transport and measurement as closely as possible to facilitate comparisons of signal intensity between measurements in different conditions. However, imprecision in the manual timing of measurements of hyperpolarized samples was unavoidable. After transport, the system was depressurized to allow used solution to be pipetted back into the bubbling vessel. The solution could then be hyperpolarized again by repressurizing it and bubbling for 30 seconds.

2.3 CPMG Measurements

CPMG measurements were done with a dwell time of 2 μs and either 256 echoes (for the regular pyridine measurements) or 512 echoes (for the hyperpolarized measurements). It was necessary to use a gain of zero (normally set to 300) for hyperpolarized CPMG measurements. (A table with a full list of parameters can be found in the appendix.) SNR was calculated in hyperpolarization measurements by comparison of the intensity of the most intense echo of a measurement with the average intensity of a measurement with no sample on the magnet and the same measurement parameters. Measurements were performed on a solution of 450 mM pyridine in deuterated water to give a reference signal level for calculation of the enhancement factor. 837 scans were needed to acquire adequate signal from the reference sample. SNR was calculated in reference measurements by comparing the intensity of the most intense echo of a measurement with the average intensity at the end of the measurement where signal has been assumed to decay to zero. This was divided by the number of scans used in the measurement to give SNR per scan. Enhancement was calculated by dividing the SNR per scan for a hyperpolarized CPMG by the SNR per scan for a reference measurement. This could be used to determine the induced polarization of the sample by multiplying the calculated thermal polarization at the magnetic field of the magnet by the enhancement factor. This strategy was also used to calculate polarization from reported enhancement values for the comparison of the constructed apparatus with other systems.

2.4 Ultrafast Measurements

Ultrafast D-T_2 pulse sequences were designed with a τ_1 of 860 μs and a τ_2 of 500 μs. Ultrafast measurements were taken with a max CHIRP power of 20 and a frequency range of 84.2 kHz, corresponding to a spatial range of 300 μm. A gain of 300 was used. A dwell time of 2 μs was used for acquisition of signal. Reference measurements to quantify the spatially-dependent sensitivity of the NMR coil were performed with a hard 180° pulse in place of the frequency sweeping CHIRP pulse, directly in the center of the τ_1 period. Hyperpolarized ultrafast measurements were taken with a single scan, and compared to a single-scan reference measurement performed on a hyperpolarized solution. Ultrafast measurements of neat pyridine were taken with 1000 scans for the signal reference measurement and 871 scans for the CHIRP measurement. Ultrafast measurements were processed with a MATLAB script which performed a Fourier transform of each echo and normalized the CHIRP measurements with the reference measurements. This data was then exported to a 2D ILT (inverse Laplace transformation) script (provided by Peter Galvosas, New Zealand) which was used to produce the D-T_2 plots.

3 Results and Discussion

3.1 Hyperpolarization

SABRE hyperpolarization was successfully performed on single-sided NMR (see Figure 13). After initial validation of the hyperpolarization apparatus with single-sided NMR was performed, the system was tuned to maximize the enhancement of signal. Measurements were compared via the SNR per scan. The number of measurements taken was limited due to evaporation of the solvent and thus loss of the hyperpolarization solution during measurement. Subsequent follow-up measurements to fill in the data were precluded due to COVID-19-related closures.

The first parameter tuned was the polarization field. SABRE hyperpolarization enhancement is highly dependent on exact matching of the J-coupling frequency to the polarization field.[21] The SNR dependence on the current sent through the solenoid was

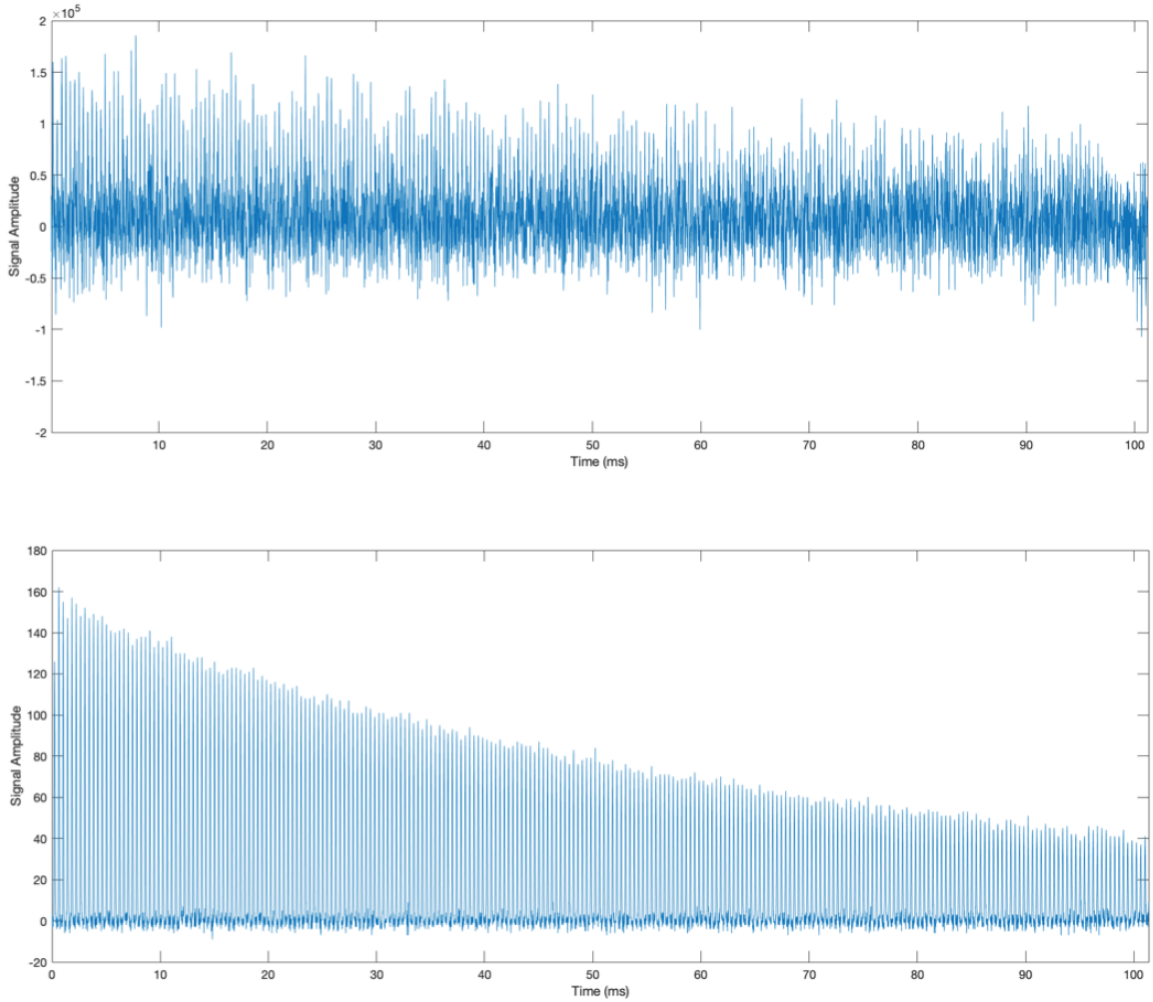

Figure 13: Above: a CPMG of regular pyridine requiring 837 signal averaged measurements to resolve. Below: a CPMG of hyperpolarized pyridine requiring only a single scan. Both samples were at a concentration of 450 mM. The hyperpolarized measurement exhibits considerable improvements in SNR and measurement time. The magnitude of values along the y axis is an artifact of how data is stored as it is signal averaged and should not be used to compare signal amplitudes between the two measurements.

measured. Current was used as the independent variable instead of the actual magnitude of the polarization field because it could be more accurately measured; however, the polarization field is expected to vary linearly with the current. Results are pictured in Figure 14. A peak is seen at a current of 342 mAmp, which was used for later measurements. Future measurements increasing resolution around this peak and verifying the reproducibility of these measurements could allow better signal enhancement.

SNR was also examined as a function of pressure. This was done to determine whether techniques aimed at dissolving more hydrogen gas in the solution (for example,

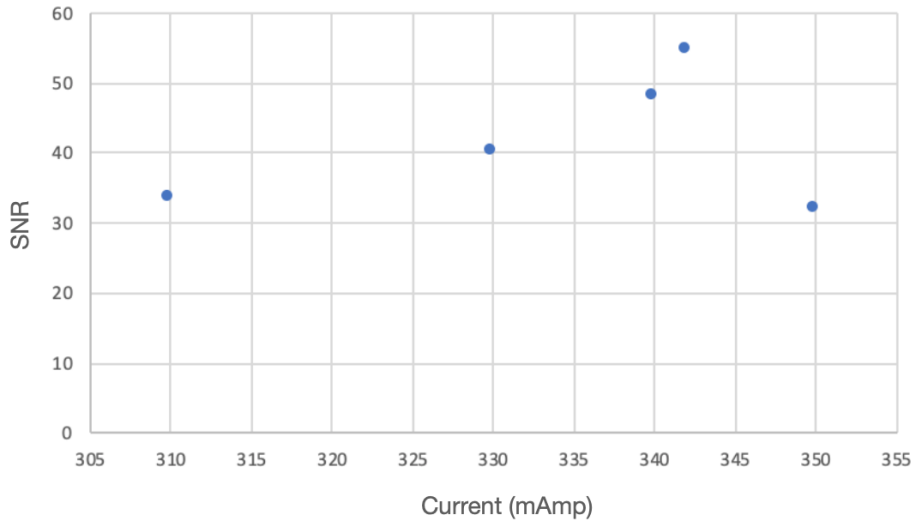

Figure 14: A plot of measured SNR against the current used to produce the polarization field.

altering the solvent to make hydrogen gas more soluble) could possibly enhance the signal. However, pressure does not influence the measured signal solely through dissolving more *para*-hydrogen enriched gas. Since the solution is transported by a pressure gradient, at higher pressures the transport time is faster, and thus the hyperpolarization has less time to decay before measurement. Results are shown in Figure 15. Since the increases in SNR with increasing pressure do not seem to level off at higher pressures, the data suggest that the enhancement factor could be improved by either improving the hyperpolarization apparatus so that it could be run at a higher pressure or by making alterations to the solvent used in the hyperpolarization solution so that it would dissolve more *para*-hydrogen gas. Naturally, the pressure is limited by the safety margins of the sample chambers.

The maximum achieved enhancement was $\epsilon = 270$, which corresponds to a polarization of about 0.027%. This was measured at a pressure of 55 psi and a current of 342 mAmp. This represents a huge improvement in signal, as pictured in Figure 13. However, a much larger polarization should be possible. Eshuis et al.[27] achieved a polarization of 0.23% using 52% enriched *para*-hydrogen gas at a pressure of 58 psi,

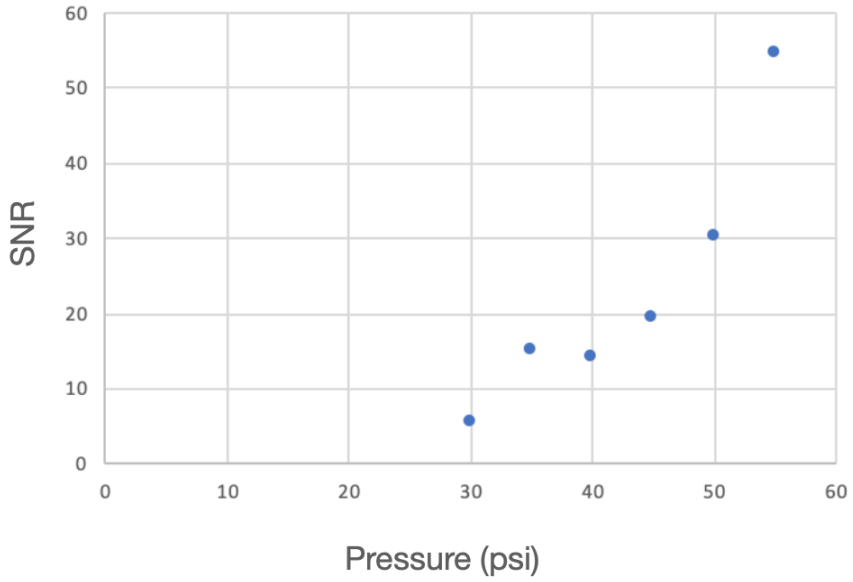

Figure 15: A plot of measured SNR against the pressure of *para*-hydrogen enriched gas used for bubbling.

very similar to the parameters of the system used here.* The higher polarization in this study may be due to a faster transfer time. However, it could also be influenced by the catalyst and pyridine concentrations used. It has been documented that lowering the pyridine:catalyst ratio and lowering the catalyst concentration lead to increases in polarization of the sample.[14,28,29] The study by Eshuis et al. used a pyridine concentration of 10 mM and a pyridine:catalyst ratio of 12.5:1 in order to achieve their polarization, which is substantially different from the concentrations here. This same effect was demonstrated by the difference in hyperpolarization solutions used in high-field and low-field NMR in this study. It is notable that the maximum polarization achieved on high-field NMR ($\epsilon \approx 0.03\%$), where a lower pressure and less exact J-coupling field were used, is approximately the same as the maximum polarization on low-field NMR, suggesting that the lower catalyst concentration used for the low-field experiments had a large effect on the observed polarization. While this pathway to improved performance should certainly be

*While hyperpolarization performance is often reported in terms of enhancement factor (ϵ), polarization is used for comparison here. The enhancement factor is highly dependent on the magnetic field strength of the magnet used, and thus not a good method for comparison of performance between studies using magnets with different field strengths. Polarization is independent of these effects, and thus better for comparisons between studies.[14]

explored, it may not lead to increased signal. In order to decrease the pyridine:catalyst ratio or to decrease the catalyst concentration with a constant ratio, the concentration of pyridine (the substrate) must decrease. This leads to reduction in signal, due to the lower concentration of sample protons. If the increase signal due to improved polarization is not larger than the decrease in signal due to a lower concentration, no net signal gain will be achieved, even if there is a larger enhancement.

Another major limitation to achieving high levels of polarization with our setup is the use of liquid nitrogen for *para*-hydrogen enrichment, which only enriches to about 52% *para*-hydrogen, as opposed to liquid helium, which is able to enrich to nearly 100%. The use of more enriched hydrogen gas results in much greater signal enhancement because it allows more of the dissolved gas to be used in hyperpolarization. Cowley et al.[28] achieved a polarization of 0.9% with nearly 100% *para*-hydrogen gas at a pressure of 44 psi with a pyridine concentration of 100 mM and a pyridine:catalyst ratio of 10:1. This is almost three times the polarization achieved in the study done by Eshuis et al., despite the fact that they were using a lower hydrogen pressure and a higher catalyst concentration. While some of this effect could be due to the smaller pyridine:catalyst ratio used here, the difference between the two ratios is small. The most important effect is the *para*-hydrogen enrichment, which allows Cowley et al. to achieve a better polarization despite a less favorable pressure and concentration. This demonstrates the power using liquid helium for *para*-hydrogen conversion. In systems using liquid helium cooling and with optimization of other parameters, polarizations on the order of 11.2% have been reported.[28] Unfortunately, liquid helium is expensive and difficult to handle and store.

The system could also be improved by increasing the safe operating pressure. As shown in Figure 15, there is a demonstrated potential for better polarization if more hydrogen gas can be dissolved in the solution. The most direct way to do this would be increasing the maximum safe pressure of the system. The pressure of the system currently is limited by the seal of the lid to teflon tubing exiting the pressure vessels. These seals begin to leak noticeably above pressures of 60 psi. However, if these seals could be improved, there is the potential to raise the operating pressure of the system

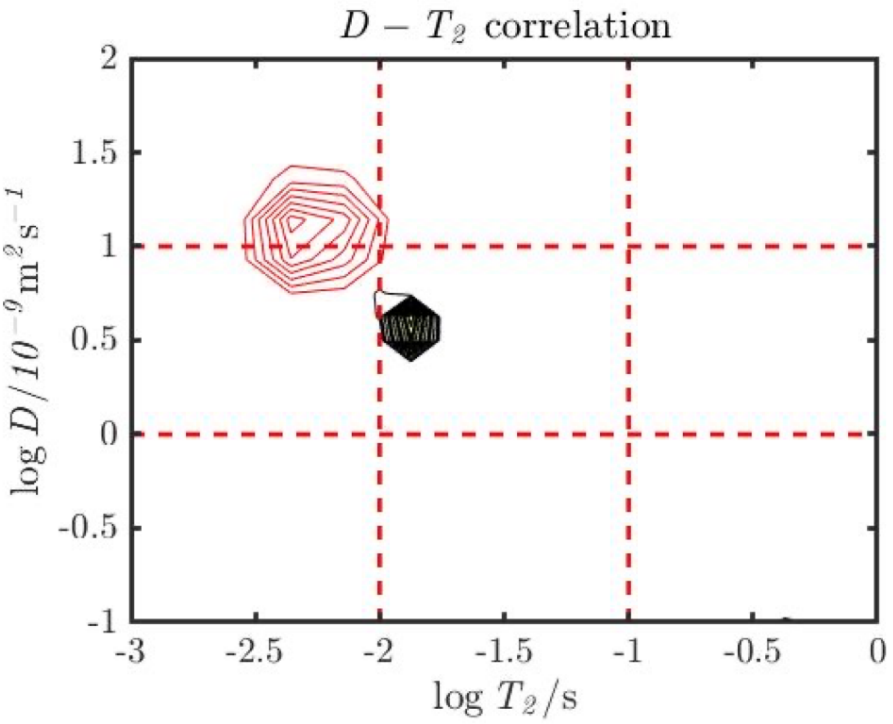

Figure 16: D-T_2 plot of hyperpolarized and neat pyridine produced from ultrafast measurements. Hyperpolarized pyridine is shown in red and neat pyridine is shown in black.

up to 150 psi, the pressure rating of the glass pressure vessels. The amount of hydrogen gas dissolved in the solution could also be improved by altering the solvent used during hyperpolarization to make hydrogen gas more soluble in the solution at a given pressure.

3.2 Ultrafast Hyperpolarization

Ultrafast D-T_2 measurements were taken of both neat pyridine and hyperpolarized pyridine, and processed to yield D-T_2 maps. Results are shown in Figure 16. The error around the neat pyridine peak is much smaller than that of the hyperpolarized pyridine peak because the SNR for measurements of hyperpolarized pyridine was limited to what could be achieved in a single scan. For neat pyridine, scans could be done successively and signal-averaged to increase SNR.

Neat pyridine was measured to have a T_2 of 46 ± 1 ms using a CPMG. The diffusion coefficient of pyridine is reported to be 1.85×10^{-9} m^{2}s^{-1}.[30] For the measurements of neat pyridine, the ultrafast measurements yielded a T_2 of approximately 21.5 ms and a D of approximately 3.16×10^{-9} m^{2}s^{-1}. For the measurements of neat pyridine, the

ultrafast measurements yielded a T_2 of approximately 5 ms and a D of approximately 1.26×10^{-9} m^2s^{-1}. The much shorter measured T_2 times in the ultrafast measurements compared to the CPMG measurements are not concerning. Ultrafast measurements are known to produce shorter T_2 times than CPMG measurements.[15] Both D and T_2 are larger for the hyperpolarized sample. This could be caused by the different environments that the two pyridine samples experience. The regular sample is of neat pyridine, but the hyperpolarized pyridine is a dilute solution in methanol. The hyperpolarized measurement is not measuring self-diffusion of pyridine, it is measuring the diffusion coefficient of pyridine in methanol. Solvent effects might also play a role in T_2 relaxation. This could be tested by measuring the T_2 of a dilute solution of pyridine in deuterated methanol and comparing this measurement to existing data for neat pyridine. Traditional diffusion measurements could also be done on a dilute solution of pyridine in deuterated methanol, but due to the low signal of this sample, the experiment would be very time-consuming. Additionally the method of sample transport may have an effect on the fluid dynamics in the sample as it is measured. The sample is transported abruptly and forcefully into the measurement beaker. It is possible that there is still some mixing or motion induced by the transport mechanism that is still present when the measurement is taking place. This motion could artificially increase the measured D and T_2. This could be tested by performing ultrafast measurements of pyridine while it is being mixed (the existing transport system could be used to agitate the solution by bubbling gas through it) and comparing those measurements to quiescent pyridine.

4 Future Directions

The development of this low-cost system for SABRE hyperpolarization for single-sided NMR has opened up the possibility of several new research directions that could be pursued. While further testing of the system is needed to understand the discrepancies between T_2 and D for regular and hyperpolarized pyridine, after this issue has been resolved, the system has the potential to expand measurement and research capabilities. In this section I will briefly discuss a few alterations that may need to be made to the

hyperpolarization apparatus to make it compatible with specific applications. I will then discuss current areas of research that might benefit from this new measurement setup.

4.1 General Improvements

4.1.1 Catalyst Separation

One major hurdle to studying systems using SABRE hyperpolarization is that the hyperpolarization catalyst must be present in the system you are measuring, either because the system is hyperpolarized directly, or because the hyperpolarization solution is injected into the system of interest, carrying the catalyst with it. The SABRE catalyst is not well studied and could interact with the system, interfering with the behavior of interest. Iali et al.[31] have proposed a solution. The hyperpolarized substrate could be separated from the catalyst using phase-transfer catalysis. In this scenario, two solvents are used: one in which both the catalyst and substrate are soluble, and one in which only the substrate is soluble. To initiate polarization transfer, the system is shaken to emulsify the two solvents, allowing the substrate and the catalyst to interact. The solvents are then allowed to settle out, separating the substrate and catalyst into the two separate phases. Iali et al. obtained reasonable polarization enhancements using deuterated chloroform and deuterated saline water as their solvents. The major issue with this setup is the time it takes for the two solvents to separate, as signal decays exponentially during this time, since the hyperpolarization is no longer being produced due to the lack of interactions between the substrate and the catalyst. Iali et al. had the best results with saline deuterated water (as opposed to pure deuterated water) which cut down the separation time from 60s to 10s. With the relatively short T_1 of pyridine this is still a major issue, as most of the signal will have decayed after 10s. However, this technique can still be useful if the level of initial polarization is high enough that there is still an enhancement after the separation time. Furthermore, it is not necessary to wait for total separation of the two solvents, as a reduction in catalyst concentration can occur if partial separation is used.

The existing hyperpolarization apparatus could be adapted to be compatible with

this technique fairly easily. The bubbling apparatus could be adapted so that the tubing used to transfer sample to the magnet draws sample from the top of a solution instead of from the bottom. Ideally, the height of the tubing would be adjustable, but this might be difficult to implement. Bubbling could be used to emulsify the two solvents, and then turned off to allow separation of the solvents. After the desired degree of separation occurs, the tubing could be used to transfer solution from the top phase for measurement. The pressure differential method of sample transfer would still be effective, as pressure could be retained in the pressure vessel by closing the flowmeter outlet when the bubbling is turned off. This would allow the built-up pressure to drive the sample transfer.

4.1.2 Hyperpolarization in Water

The system could also be improved by adapting it to perform hyperpolarization in deuterated water. Many systems, especially biological systems, need to be investigated in an aqueous environment. Furthermore, deuterated water is a much more cost-effective solvent than deuterated methanol. It has been shown that the SABRE catalyst used in this study can be adapted for use in aqueous environments.[32] This can be done by activating the catalyst first in an organic solvent, which is then boiled away, leaving behind the activated catalyst (cyclooctadiene unit removed). After the catalyst is activated it becomes water soluble, so the dried catalyst can then be dissolved in water and used for hyperpolarization. Successful SABRE hyperpolarization has been demonstrated using this technique.

This technique would be fairly easy to adapt to our system. The pressure vessel used for hyperpolarization could be used for the initial activation of the catalyst. Methanol (which is much less expensive than deuterated methanol) could be used during the activation step, and then thoroughly removed during the evaporation step to increase the cost-effectiveness of the system. However, switching to water as a solvent would almost certainly lead to lower hyperpolarization, since hydrogen gas is much less soluble in water than in methanol.[32] Therefore, at the same pressure, much less hydrogen gas would dissolve into the hyperpolarization solution, which would reduce the amount of hyperpolarization that could occur. These effects could be mitigated by other improvements

to the system promoting hyperpolarization or by using a solvent which is a mixture of deuterated methanol and deuterated water.

4.1.3 Hyperpolarization of Other Substrates

Another major limitation of the current hyperpolarization setup is that it has only been adapted for hyperpolarization of pyridine. While the SABRE catalyst used here has shown to be effective for species with multiple bonds to nitrogen,[20] hyperpolarization of other substrates is necessary for the system to be effective for many applications. A technique has been developed, termed "SABRE-RELAY", where ammonia is directly hyperpolarized using the SABRE catalyst, and then transfers its polarization to other species in solution.[20] This occurs through a combination of proton exchange and intramolecular interactions between nuclei. This technique has proved to be effective for a variety of molecules, including amines, amides, carboxylic acids, alcohols, phosphates, and carbonates. The technique would require some alterations to be performed on single-sided NMR. In high-field NMR, distinguishing the signal of the hyperpolarized substrate from hyperpolarized ammonia is possible due to chemical shift detection. However, this is impossible with single-sided NMR, as discussed previously. Thus, this could only be used in situations where the signal from the ammonia and the substrate could be distinguished. This could be done via ultrafast D-T_2 measurements, if D and T_2 were sufficiently different between the two substances. This also could possibly be done in a simple CPMG if the T_2 of the substances were sufficiently different by performing a biexponential fit of the decay.

Another species of interest for hyperpolarization is water. Water is biocompatible, and can be used to probe a variety of behaviors by measurement of its interactions with other substances.[3,33] This has been achieved through the use of a water-soluble SABRE catalyst* used in tandem with L-histidine in mixtures of water and deuterated water.[34] This technique requires heating the hyperpolarization solution to 90°C during bubbling to promote fast exchange at the catalyst. In order for this technique to be performed on the existing apparatus, alterations would need to be made to allow heating of the

*IrCl(IDEG)(COD) where IDEG = 1,3-bis(3,4,5-tris(diethyleneglycol)benzyl)imidazole-2-ylidene

bubbling apparatus. This would likely require a completely re-designed solenoid mount, since the existing mount relies on 3D printed plastic, which melts easily. This heating would also need to be taken into account when determined safe maximum pressures of the bubbling vessel. Furthermore, the new catalyst would either need to be synthesized in-house or a reliable source for the catalyst would need to be found.

4.2 Applications

4.2.1 Small Molecule Penetration

Hyperpolarization could be useful in probing small molecule penetration through membranes or into polymers. A particular system of interest is oil paints. Oil paintings require cleaning and varnish removal occasionally, which is typically done with organic solvents or aqueous gels. However, these cleanings can lead to short-term swelling or long-term embrittlement of the paintings if the solvent used for cleaning penetrates into the paint film.[35,36] Single-sided NMR is particularly well-suited for the detection of solvent penetration because of its field gradient, which allows depth profiling through a sample. Previous unpublished research from the Meldrum lab has demonstrated the ability of single-sided NMR to detect large-scale solvent penetration into paint films over long periods of time. However, before solvent penetration can be detected, a large amount of solvent must accumulate in the paint film.

Detection of solvent penetration into a polymer requires that the signal generated by the solvent be comparable to that generated by the polymer protons. If hyperpolarization provides enough enhancement of solvent signal to meet this condition at lower concentrations of solvent, hyperpolarization could allow detection of small amounts of solvent penetration into the paint film over a short period of time, which is more accurate to the actual conditions a painting is exposed to during cleaning. This technique would be limited in that it would not give information on the concentration of solvent in the paint film. Since hyperpolarization artificially increases the signal generated from a substance, the measured signal intensity of a hyperpolarized substance is no longer proportional to its concentration. This could possibly be circumvented if the behavior

of the hyperpolarization apparatus were extremely well-characterized. However, even if the amount of solvent penetrating into paint films was unknown, this technique could still provide valuable data. Signal from the solvent would serve as a binary indication of the solvent's presence, and could be used to determine the depth of penetration via depth profiling. This data could be compared with measurements of paint samples after they are allowed to recover to determine the long-term effects of instantaneous solvent penetration into paint films.

In order to perform this research, the system would have to be adapted to hyperpolarize solvents of interest. Both water and methanol have been successfully hyperpolarized previously, and are solvents of interest. The test setup would also need to be adjusted so that controlled dosages of hyperpolarized substrate could be deposited on a paint film. This could be done by limiting sample flow out of the bubbling vessel using a needle valve. Furthermore, an ideal test setup would allow separation of the catalyst from the hyperpolarized solvent, since effects of the catalyst on the paint film are not of interest.

This technique could also be extended to other, similar systems where small molecule penetration is of interest. For example, there is some interest in measuring the diffusion characteristics of water through nafion membranes for use in improving fuel cells.[37,38] While extensive research has already been performed in this area, hyperpolarization may allow novel measurements of instantaneous effects. Furthermore, the open geometry of single-sided NMR may allow novel measurements of a fuel cell in operation. However, collaboration or correspondence with an expert in these membranes would be necessary for this type of study due to the expertise required to understand the extensive research that has been performed in this area.

4.2.2 Protein Binding

Previous research has established the capability of single-sided NMR to probe protein-ligand interactions via ultrafast D-T_2 measurements.[3] This is desireable because the low-cost setup of single-sided NMR (as opposed to high-field NMR) makes these measurements more accessible. Furthermore, with the open geometry of single-sided NMR, these types of measurements could be performed on planar systems, such as biofilms.

However, a major hurdle in the study was the required measurement time to resolve signal. In order to shorten measurement times to practical lengths, measurement parameters (specifically the number of echoes) had to be compromised. Even with shortened measurement times, measurements still took hours to complete. This lead to potential errors due to degradation of the sample over time.

This type of experiment could be greatly improved with hyperpolarization. If ligands can be found which are compatible with hyperpolarization, similar studies can be performed on a much faster time scale with hyperpolarized D-T_2 measurements similar to the measurements demonstrated in this study. This lowers the cost of instrumentation necessary to study protein-ligand interactions, and allows for possible measurements of these interactions in planar systems, such as biofilms or organ-on-a-chip systems. However, this technique is limited by the T_1 of the hyperpolarized ligand. If the protein-ligand interactions take longer to occur than the T_1 relaxation of the hyperpolarized ligand, this will be an ineffective technique.

5 Molecular Dynamics

This section is unrelated to the development and testing of the SABRE hyperpolarization apparatus. It has been included to document additional research occurring during the honor's research period as well as to provide a record of the procedures developed for future research.

5.1 Introduction

Effort has been made to develop a molecular dynamics research program to supplement experimental measurements of epoxy interfaces. The goal is to develop software that will allow the simulation of interfaces to generate NMR parameters (T_1, T_2) which can then be compared to experimental measurements. By tailoring the simulations to match experimental results, a better understanding can be gained of the interactions occurring at the interfaces. However, simulation parameters for epoxy interfaces are quite complex and difficult to generate. Proof-of-concept measurements for water and cyclohexane,

much simpler systems, were selected as initial goals for the research program.

Molecular dynamics simulations in this study were done using Nanoscale Molecular Dynamics (NAMD)*, which was selected due to its abilities to handle complex systems efficiently through GPU processing. Molecular dynamics simulations function by computing the potential energy experienced by each atom in the system and using these values to calculate motion of the system over time. The potential energy is determined by force field parameters which describe how specific types of atoms will interact with the rest of the system. These parameters describe components of the potential energy that an atom will experience or produce, for example, one term deals with interactions due to chemical bonds between atoms. Motion is calculated in small time steps (on the order of a couple fs) but stored in much larger time steps (on the order of hundreds of ps). This allows accuracy in determining motion without placing unwieldy storage demands on the system.

Simulation boundary conditions can be set to an arbitrary shape, or the simulation can make use of periodic boundary conditions. Periodic boundary conditions are typically used with a cubic geometry, and involve "repeating" the simulation geometry out to infinity. The system will behave as though an identical system neighbors it on all sides. Atoms moving out of the cubic geometry will appear on the opposite face moving in the same direction, and atoms near the edges of the system will interact with potentials produced by atoms on the opposite site. This type of simulation is useful because it avoids surface effects.

NAMD simulations can be used to calculate NMR parameters through the trajectory (dcd) files generated in simulations. A strategy developed by Singer et al. was used here.[40] These trajectory files note the positions of atoms in the system at each time point. The autocorrelation function documents the distance between a each atom and all other relevant atoms in the system at each time point. This information is used to calculate the average intermolecular and intramolecular distances for all atoms in the

*NAMD was developed by the Theoretical and Computational Biophysics Group in the Beckman Institute for Advanced Science and Technology at the University of Illinois at Urbana-Champaign.[39]

system. These averages are used to calculate the second moment:

$$\Delta\omega_{R,T} = \frac{9}{16}\left(\frac{\mu_0}{4\pi}\right)^2 \hbar^2\gamma^4 \frac{1}{m_{R,T}^6} \tag{12}$$

where m_R is the average of intramolecular distances, m_T is the average of intermolecular distances, and $\Delta\omega_{R,T}$ describes the relevant second moment. In liquids with low viscosities, the assumption can be made that $T_1 \approx T_2$, and the following simplified equation can be derived:

$$T_1 = T_2 = \frac{1}{\frac{10}{3}\tau\left(\Delta\omega_R^2 + \Delta\omega_T^2\right)} \tag{13}$$

where τ represents the length of the simulation.

However, the assumption that $T_1 \approx T_2$ for liquids with low viscosities does not hold up in our measurements. We have measured water to have a T_1 of approximately 2.5 s and a measured T_2 of approximately 30 ms, which are very different. T_2 is highly dependent on measurement parameters, especially the echo time, in measurement setups with large field gradients, like single-sided NMR. Thus, the calculated value may more accurately match the measured T_1. These calculations will need to be adapted to provide a more accurate representation of our measurement setup, but they are suitable for initial testing of the simulations.

5.2 Methods

Developing force field parameters for non-biological systems is somewhat difficult when using NAMD, since NAMD was created specifically to be used with biomolecules. NAMD is set up by default to use CHARMM parameters, which assume a substance is made up of amino acid subunits, and use these to define the force field parameters. This does not work for systems of simple organic molecules, like cyclohexane. To simulate simple organic molecules in NAMD, suitable force field parameters need to be imported. Furthermore, the structure files describing the system to be simulated need to be set up so they are compatible with the force field being used.

For use in our system, the General Amber Force Field (GAFF) was selected.[41] GAFF is designed to generate parameters for small organic molecules based on the behavior of individual atoms in a given environment (for example, there might be parame-

ters for a CH_3 carbon and a CH_2 carbon). Thus it is ideal for calculating parameters for molecules such as cyclohexane. Theoretically, it could also be used to generate parameters for more complex systems, such as an epoxy surface. GAFF parameters were correlated with our simulation systems using AmberTools18.[42] This procedure was developed with the aid of published tutorials, which are linked in the bibliography.[43,44]

To generate parameters for a box filled with a particular molecule, a structure for a single molecule was initially designed in Avogadro.[45] Avogadro was selected due to its ease in handling 3D structures and its simple structure relaxation capabilities. The single molecule structure was relaxed and then saved as a pdb file. However, alterations needed to be made to the pdb file to make it compatible with Amber processing software. These alterations were done by hand using a simple text editor. "HETATOM" entries were changed to "ATOM" entries, and atom names were altered to make each one unique (ie. "C" would be changed to "C1" etc. for each carbon atom in the molecule). These alterations were made taking care to preserve the necessary spacing conventions for the pdb file. After alterations were made to the pdb file, it was converted to a mol2 file using antechamber (in AmberTools18). This could easily be done using commands in the terminal (see Listing 3 in the Appendix). After attempting to convert a pdb file, it was important to check the generated sqm.out file to ensure that calculations had converged. The generated mol2 file was examined using a text editor to ensure that the atom types assigned for each atom in the molecule made logical sense. Next, the parmchk program (in AmberTools18) was used to check that the mol2 file had sufficient parameters to describe all atoms. In the case where the molecule did not have the necessary parameters, this would be noted in an output frcmod file. The frcmod file can be used to note necessary alterations to the GAFF force field in a simulation. Amber will attempt to calculate parameters for some atoms, even if it does not have parameters for them, and this will be noted in the file. Ideally, these parameters should be verified by additional simulations. For the molecules used in initial testing, no problems with parameters were noted in these files.

The initially generated pdb files were then used to generate a simulation geometry in packmol (see Listing 5 in the Appendix). This allowed for the random placement of

molecules within a defined volume, subject to energetic considerations. The number of molecules that should be used in a given volume was determined from the density of the substance at room temperature. Then, tLEaP (from AmberTools18) was used to generate Amber input files from the simulation geometry pdb generated from packmol, and the mol2 files generated previously. It is also important to note that tLEaP outputs the dimensions of the simulation geometry after a successful run, which is important for setting up NAMD simulations.

NAMD simulations were run on boxes of water and cyclohexane generated using these parameters (scripts in the Appendix). Initially a short equilibration simulation was run to minimize energy due to interactions between molecules and to set the temperature. Then, restart files generated from the equilibration were used to run a longer simulation at constant temperature and pressure. The autocorrelation function was processed using an in-house MATLAB script based on work by Singer et al.,[40] discussed earlier. While parameters were developed for cyclohexane, the MATLAB script was only used to process data from measurements of water, due to limitations of the current processing algorithm.

5.3 Results and Discussion

Results from the simulations of water parametrized by the GAFF force field were processed to calculate T_1 and T_2 for the system. The simulation returned a value of 0.85 s, which does not agree with either the measured T_1 of water (approximately 2.5 s) or the measured T_2 of water (approximately 30 ms). The disagreement in the values could be a result of the simplifications made in calculations. However, they could also be due to inaccuracy in the force field parameters for water used in the simulation. While the GAFF force field is generally accurate for many small organic molecules, it is conventional to use water-specific parameters for simulations of water. Previous work has shown TIP4P/2005 water model is suitable for calculating NMR parameters,[40] and it is available within AmberTools18.

5.4 Future Directions

Procedures for using an Amber-compatible water model need to be developed. While there are existing TIP4P/2005 water parameters included in AmberTools18, initial attempts to implement them have been unsuccessful due to persistent, unresolved syntax problems which prevent the software from correctly assigning force field parameters to atoms in the structure files. More work will be needed to resolve these issues. Furthermore, the in-house MATLAB script developed to process simulations will need to be expanded so it can better calculate relaxation values and handle molecules like cyclohexane, which have many hydrogen nuclei that need to be accounted for. Once simulations of pure water and pure cyclohexane agree with experimental data, simulations of water and cyclohexane interfaces will need to be developed and validated.

6 References

[1] N. A. Udell, R. Hodgkins, B. H. Berrie, and T. Meldrum, "Physical and chemical properties of traditional and water-mixable oil paints assessed using single-sided nmr," *Microchemical Journal*, vol. 133, pp. 31–36, July 2017.

[2] N. Halmen, C. Kugler, E. Kraus, B. Baudrit, T. Hochrein, and M. Bastian, "Single-sided nmr for the measurement of the degree of cross-linking and curing," *Journal of Sensors and Sensor Systems*, vol. 7, pp. 21–30, 2018.

[3] J. Gray, "Diffusion-based biomolecular sensing using low-field nmr," *Undergraduate Honors Theses*, p. Paper 132, May 2015.

[4] P. Moretti, L. Cartechini, and C. Miliani, "Single-sided nmr: a non-invasive diagnostic tool for monitoring swelling effects in paint films subjected to solvent cleaning," *Analytical and Bioanalytical Chemistry*, vol. 412, pp. 106–1075, February 2020.

[5] N. Marigheto, L. Venturi, and B. Hills, "Two-dimensional nmr relaxation studies of apple quality," *Postharvest Biology and Technology*, vol. 48, pp. 331–340, June 2008.

[6] N. Marigheto, S. Duarte, and B. Hills, "Nmr relaxation study of avocado quality," *Applied Magnetic Resonance*, vol. 19, pp. 687–701, December 2005.

[7] R. L. Kleinberg and J. A. Jackson, "An introduction to the history of nmr well logging," *Concepts in Magnetic Resonance*, vol. 13, pp. 340–342, June 2001.

[8] M. Kelley, N. Abdol, P. Soroushian, K. Keating, A. M. Balachandra, and T. Meldrum, "Monitoring real-time curing of epoxies in situ using single-sided nmr," *Journal of Polymer Science*, vol. 58, pp. 616–623, January 2020.

[9] M. Brass, F. Morin, and T. Meldrum, "Spatially resolved measurements of crosslinking in uv-curable coatings using single-sided nmr," *Magnetochemistry*, vol. 4, p. 8, 2018.

[10] M. Barbieri, L. Brizi, V. Bortolotti, P. Fantazzini, M. Nogueira d'Eurydice, S. Obruchkov, K. Liu, and P. Galvosas, "Single-sided nmr for the diagnosis of osteoporosis: Diffusion weighted pulse sequences for the estimation of trabecular bone

volume fraction in the presence of muscle tissue," *Microporous and Mesoporous Materials*, vol. 269, pp. 166–170, October 2018.

[11] M. C. Tourell, T. S. Ali, H. J. Hugo, C. Pyke, S. Yang, T. Lloyd, E. Thompson, and K. Momot, "t_1-based sensing of mammographic density using single-sided portable nmr," *Magnetic Resonance in Medicine*, vol. 80, pp. 1243–1251, February 2018.

[12] M. E. Halse, "Perspectives for hyperpolarisation in compact nmr," *TrAC Trends in Analytical Chemistry, Part 1*, vol. 83, pp. 76–83, October 2016.

[13] J. H. Lee, Y. Okuno, and S. Cavagnero, "Sensitivity enhancement in solution nmr: emerging ideas and new frontiers," *Journal of Magnetic Resonance*, vol. 241, pp. 18–31, April 2014.

[14] R. E. Mewis, "Developments and advances concerning the hyperpolarisation technique sabre," *Magnetic Resonance Chemistry*, vol. 53, pp. 789–800, 2015.

[15] J. N. King, A. Fallorina, J. Yu, G. Zhang, V. Telkki, C. Hilty, and T. Meldrum, "Probing molecular dynamics with hyperpolarized ultrafast laplace nmr using a low-field, single-sided magnet," *Chemical Science*, vol. 9, pp. 6143–6149, July 2018.

[16] J. Keeler, *Understanding NMR Spectroscopy*. Wiley, 2010.

[17] M. H. Levitt, *Spin Dynamics: Basics of Nuclear Magnetic Resonance*. Wiley, 2008.

[18] H. Carr and E. M. Purcell, "Effects of diffusion on free precession in nuclear magnetic resonance experiments," *Physical Review*, vol. 94, pp. 630–638, May 1954.

[19] S. Meiboom and D. Gill, "Modified spin-echo method for measuring nuclear relaxation times," *Review of Scientific Instruments*, vol. 29, pp. 688–691, August 1958.

[20] W. Iali, P. J. Rayner, and S. B. Duckett, "Using *para*hydrogen to hyperpolarize amines, amides, carboxylic acids, alcohols, phosphates, and carbonates," *Science Advances*, vol. 4, 2018.

[21] D. A. Barskiy, S. Knecht, A. V. Yurkoskaya, and K. L. Ivanov, "Sabre: Chemical kinetics and spin dynamics of the formation of hyperpolarization," *Progress in Nuclear Magnetic Resonance Spectroscopy*, vol. 114-115, pp. 33–70, October 2019.

[22] B. J. A. van Weerdenburg, S. Glöggler, N. Eshuis, A. H. J. Engwerda, J. M. M. Smits, R. de Gelder, S. Appelt, S. S. Wymenga, M. Tessari, M. C. Feiters, B. Blümich, and T. P. J. T. Rutjes, "Ligand effects of nhc-iridium catalysts for signal amplification by reversible exchange (sabre)," *Chemical Communications*, vol. 49, pp. 7388–7390, June 2013.

[23] A. N. Pravdivtsev, A. V. Yurkovskaya, I. K. L. Vieth, H.-M., and R. Kaptein, "Level anti-crossings are a key factor for understanding *para*-hydrogen-induced hyperpolarization in sabre experiments," *ChemPhysChem*, vol. 14, pp. 3327–3331, 2013.

[24] D. A. Barskiy, A. N. Pravdivtsev, K. L. Ivanov, K. V. Kovtunov, and I. V. Koptyung, "A simple analytical model for signal amplification by reversible exchange (sabre) process," *Physical Chemistry Chemical Physics*, vol. 18, pp. 89–93, 2016.

[25] T. Katayama and T. Nitta, "Solubilities of hydrogen and nitrogen in alcohols and *n*-hexane," *Journal of Chemical and Engineering Data*, vol. 21, 1976.

[26] G. R. Fulmer, A. J. M. Miller, N. H. Sherden, H. E. Gottlieb, A. Nudelman, B. M. Stolz, J. E. Bercaw, and K. I. Goldberg, "Nmr chemical shifts of trace impurities: Common laboratory solvents, organics, and gases in deuterated solvents relevant to the organometallic chemist," *Organometallics*, vol. 29, pp. 2176–2179, 2010.

[27] N. Eshuis, N. Hermkens, B. J. A. van Weerdenburg, M. C. Feiters, F. P. J. T. Rutjes, S. R. Wijmenga, and M. Tessari, "Toward nanomolar detection by nmr through sabre hyperpolarization," *Journal of the American Chemical Society*, vol. 136, pp. 2695–2698, 2014.

[28] M. J. Cowley, R. W. Adams, K. D. Atkinson, M. C. R. Cockett, S. B. Duckett, G. R. Green, J. A. B. Lohman, R. Kerssebaum, D. Kilgour, and R. E. Mewis, "Iridium n-heterocyclic carbene complexes as efficient catalyst for magnetization transfer from

para-hydrogen," *Journal of the American Chemical Society*, vol. 133, pp. 6134–6137, April 2011.

[29] P. M. Richardson, A. J. Parrott, O. Semenova, A. Nordson, S. B. Duckett, and M. E. Halse, "Sabre hyperpolarization enables high-sensitivity ^{1}h and ^{13}c benchtop nmr spectroscopy," *Analyst*, vol. 143, pp. 3442–3450, June 2018.

[30] I. Bako, T. Radnai, and G. Palinkas, "Investigation of the structure of liquid pyridine: a molecular dynamics simulation, an rism, and an x-ray diffraction study," *Zeitschrift für Naturforschung A*, vol. 51, 2014.

[31] W. Iali, A. M. Olaru, G. G. R. Green, and S. B. Duckett, "Achieving high levels of nmr-hyperpolarization in aqueous media with minimal catalyst contamination using sabre," *Chemistry A European Journal*, vol. 23, pp. 10491–10495, 2017.

[32] M. L. Truong, F. Shi, P. He, B. Yuan, K. N. Plunkett, A. M. Coffey, R. V. Shchepin, D. A. Barsiky, K. V. Kovtunov, I. V. Koptyug, K. W. Waddell, B. M. Goodson, and E. Y. Chekmenev, "Irreversible catalyst activation enables hyperpolarization and water solubility for nmr signal amplification by reversible exchange," *The Journal of Physical Chemistry B*, vol. 118, pp. 13882–13889, 2014.

[33] Q. Chappuis, J. Milani, B. Vuichoud, A. Bornet, A. D. Gossert, G. Bodenhausen, and S. Jannin, "Hyperpolarized water to study protein-ligand interactions," *The Journal of Physical Chemistry Letters*, vol. 6, pp. 1674–1678, 2015.

[34] S. Lehmkuhl, M. Emondts, L. Schubert, P. Spannring, J. Klankermayer, B. Blümich, and P. P. M. Schleker, "Hyperpolarizing water with parahydrogen," *ChemPhysChem Communications*, vol. 18, pp. 2426–2429, 2017.

[35] A. Phenix and K. Sutherland, "The cleaning of paintings: effects of organic solvents on oil paint films," *Studies in Conservation*, vol. 46, pp. 47–60, 2001.

[36] J.-S. Tsang and D. Erhardt, "Current research on the effects of solvents and gelled and aqueous cleaning systems on oil paint films," *Journal of the American Institute for Conservation*, vol. 31, pp. 87–94, 1992.

[37] K. A. Mauritz and R. B. Moore, "State of understanding of nafion," *Chemical Reviews*, vol. 104, pp. 4535–4585, 2004.

[38] A. Kusoglu and A. Z. Weber, "New insights into perfluorinated sulfonic-acid ionomers," *Chemical Reviews*, vol. 117, pp. 987–1104, 2017.

[39] J. C. Phillips, R. Braun, W. Wang, J. Gumbart, E. Tajkhorshid, E. Villa, C. Chipot, R. D. Skeel, L. Kale, and K. Schulten, "Scalable molecular dynamics with namd," *Journal of Computational Chemistry*, vol. 26, pp. 1781–1802, 2005.

[40] P. M. Singer, D. Asthagiri, W. G. Chapman, and G. J. Hirasaki, "Molecular dynamics simulations of nmr relaxation and diffusion of bulk hydrocarbons and water," *Journal of Magnetic Resonance*, vol. 277, pp. 15–24, 2017.

[41] J. Wang, R. M. Wolfe, J. W. Caldwell, P. A. Kollman, and D. A. Case, "Development and testing of a general amber force field," *Journal of Computational Chemistry*, vol. 25, pp. 1157–1174, 2004.

[42] D. A. Case, I. Y. Ben-Shalom, S. R. Brozell, D. Cerutti, T. E. I. Cheatham, V. W. D. Cruziero, T. A. Darden, R. E. Duke, D. Ghoreishi, M. K. Gilson, H. Gohlke, A. W. Goetz, D. Greene, R. Harris, N. Homeyer, S. Izadi, A. Kovalenko, T. Kurtzman, T. S. Lee, S. LeGrand, P. Li, C. Lin, J. Liu, T. Luchko, R. Luo, D. J. Mermelstein, K. M. Merz, Y. Miao, G. Monard, C. Nguyen, H. Nguyen, I. Omelyan, A. Onufriev, F. Pan, R. Qi, D. R. Roe, A. Roitberg, C. Sagui, S. Schott, Verdugo, J. Shen, C. L. Simmerling, J. Smith, R. Salomon-Ferrer, J. Swails, R. C. Walker, J. Wang, H. Wei, R. M. Wolf, X. Wu, L. Xiao, D. M. York, and P. A. Kollman, "Amber 2018," 2018. University of California, San Francisco.

[43] R. Walker, S. Tang, M. Barton, and T. Luchko, "Antechamber tutorial: Using antechamber to create leap input files for simulating sustiva (efavirenz)-rt complex using the general amber force field." url: http://ambermd.org/tutorials/basic/tutorial4b/.

[44] C. Lim and D. A. Case, "Tutorial: A room-temperature ionic liquid." url: https://ambermd.org/tutorials/advanced/tutorial15/Tutorial2.xhtml.

[45] M. D. Hanwell, D. E. Curtis, D. C. Lonie, T. Vandermeersch, E. Zurek, and G. R. Hutchison, "Avogadro: An advanced semantic chemical editor, visualization, and analysis platform," *Journal of Cheminformatics*, vol. 4, 2012.

[46] E. Kupce and R. Freeman, "Adiabatic pulses for wideband inversion and broadband decoupling," *Journal of Magnetic Resonance, Series A*, vol. 115, pp. 273–276, 1995.

7 Appendix

7.1 NMR Measurement Parameters

CPMG Measurement Parameters	
dwell time	2 μs
number of acquisition points	32
acquisition time (per echo)	64 μs
number of scans	varies
Rx gain	300 (regular) or 0 (hyperpolarized)
90° pulse power	1.47 mT
180° pulse power	2.94 mT
hard pulse length	4 μs
number of echoes	256 (regular) or 512 (hyperpolarized)
repetition time	12s
echo time	200 μs

Table 2: Measurement parameters for the CPMG experiments used in this study.

Ultrafast Measurement Parameters	
dwell time	2 μs
number of acquisition points	78
acquisition time (per echo)	156 μs
number of scans	varies
Rx gain	300
90° pulse power	1.47 mT
180° pulse power	2.94 mT
hard pulse length	4 μs
CHIRP pulse length	427.8 μs
max CHIRP power	1.05 mT
CHIRP amplitude shape	WURST*
τ_1	860 μs
τ_2	500 μs
number of echoes	128
repetition time	15s
echo time	300 μs

Table 3: Measurement parameters for the ultrafast measurements used in this study.

*For more information on the WURST pulse shaping, see Kupce et al.[46]

7.2 Molecular Dynamics Scripts and Procedures

Listing 1: Example pdb (of a single water molecule) file before manual editing.

```
COMPND    UNNAMED
AUTHOR    GENERATED BY OPEN BABEL 2.3.90
HETATM    1  O   HOH     1       -0.943   1.524   0.000  1.00  0.00           O
HETATM    2  H   HOH     0        0.027   1.524   0.000  1.00  0.00           H
HETATM    3  H   HOH     0       -1.267   2.431   0.122  1.00  0.00           H
CONECT    1    2    3
CONECT    2    1
CONECT    3    1
MASTER        0    0    0    0    0    0    0    0    3    0    3    0
END
```

Listing 2: Example pdb (of a single water molecule) file after manual editing.

```
COMPND    UNNAMED
AUTHOR    GENERATED BY OPEN BABEL 2.3.90
ATOM      1  O   UNL     1       -0.943   1.524   0.000  1.00  0.00           O
ATOM      2  H1  UNL     0        0.027   1.524   0.000  1.00  0.00           H
ATOM      3  H2  UNL     0       -1.267   2.431   0.122  1.00  0.00           H
CONECT    1    2    3
CONECT    2    1
CONECT    3    1
MASTER        0    0    0    0    0    0    0    0    3    0    3    0
END
```

Listing 3: An example of the terminal commands used to convert a pdb file to a mol2 file using antechamber.

```
antechamber -i molecule_name.pdb -fi pdb -o molecule_name.mol2 -fo mol2 -c bcc -s 0
```

Listing 4: Example mol2 file (of a single water molecule) generated by antechamber. Note the atom types listed in the fifth column in the second section which can be used to verify that the correct parameters were assigned.

```
@<TRIPOS>MOLECULE
UNL
    3     2     1     0     0
SMALL
bcc


@<TRIPOS>ATOM
      1 O            -0.9430     1.5240     0.0000 oh          1 UNL       -0.785000
```

```
10       2 H1            0.0270      1.5240      0.0000 ho          0 UNL        0.392000
11       3 H2           -1.2670      2.4310      0.1220 ho          0 UNL        0.392000
12 @<TRIPOS>BOND
13      1      1      2 1
14      2      1      3 1
15 @<TRIPOS>SUBSTRUCTURE
16      1 UNL          1 TEMP               0 ****  ****     0 ROOT
```

Listing 5: Example code used to generate simulation geometries in packmol. The input pdb file (wat.pdb) was generated earlier using avogadro and edited manually. Line 7 sets the number of molecules used, while line 8 sets the volume and position of the box where the molecules are placed (using units of Angstroms).

```
1 tolerance 2.0
2 filetype pdb
3
4 output 26_Feb_wat/26_Feb_wat.pdb
5
6 structure 26_Feb_wat/wat.pdb
7   number 512
8   inside box 0. 0. 0. 25 25 25
9 end structure
```

Listing 6: Example command input to tLEaP to generate the Amber input files used in NAMD. The GAFF force field is imported in line 2. In line 3 the mol2 file generate for water is loaded. In line 4, the pdb for the system is loaded and assigned to the variable name "interface." Line 6 imports corrections to the force field generated by parmck2 (in this case the file is empty). The command on line 7 sets the geometry for the output system. The command on line 8 generates the input Amber files necessary for NAMD simulations.

```
1 # change location of files accordingly
2 source leaprc.gaff
3 wat = loadmol2 wat.mol2
4
5 interface = loadPdb big_box.pdb
6 loadamberparams frcmod.wat
7 setbox interface centers
8 saveAmberParm interface big_box.prmtop big_box.inpcrd
```

Listing 7: Example NAMD .conf file used to run a simulation. A modified version of this script was used to run minimizations: temperature was used instead of the restart files in the input section, a shorter run time was used, and the simulation would write to the dcd less frequently. This would generate the restart files to be used in the simulation.lst:conf

```
#############################################################
## JOB DESCRIPTION                                         ##
#############################################################

# Minimization and Equilibration of
# a box of water

#############################################################
## ADJUSTABLE PARAMETERS                                   ##
#############################################################

# Amber/(t,s,x)leap generated parm and crd file
parmfile    big_box/big_box.prmtop
ambercoor   big_box/big_box.inpcrd

set temperature     293

set outputname      big_box/17Feb

firsttimestep       0

#############################################################
## SIMULATION PARAMETERS                                   ##
#############################################################

# INPUT
bincoordinates  big_box/17Feb.restart.coor
binvelocities   big_box/17Feb.restart.vel
extendedSystem  big_box/17Feb.restart.xsc
amber on
#temperature $temperature

#Force-Field Parameters
exclude         scaled1-4
1-4scaling      1.0
cutoff          12.0
switching       on #this could be a problem
switchdist      10.0
pairlistdist    14.0

# Integrator Parameters
timestep            2.0  ;# 2fs/step
rigidBonds          all  ;# needed for 2fs steps, could be a problem for NMR sims
nonbondedFreq       1
fullElectFrequency  2
stepspercycle       10
```

```
47
48 # Constant Temperature Control
49 langevin            on    ;# do langevin dynamics
50 langevinDamping     1     ;# damping coefficient (gamma) of 1/ps
51 langevinTemp        $temperature
52 langevinHydrogen    off    ;# don't couple langevin bath to hydrogens
53
54 # Periodic Boundary Conditions
55 cellBasisVector1     43.2   0.0   0.0
56 cellBasisVector2     0.0   43.3  0.0
57 cellBasisVector3     0.0    0     43.3
58 cellOrigin           21.6  21.65  21.65
59
60 wrapAll             on
61
62
63 # PME (for full-system periodic electrostatics)
64 PME                 yes
65 PMEGridSpacing      1.0
66
67 #manual grid definition
68 #PMEGridSizeX        45
69 #PMEGridSizeY        45
70 #PMEGridSizeZ        48
71
72 # Constant Pressure Control (variable volume)
73 useGroupPressure      yes ;# needed for rigidBonds
74 useFlexibleCell       no
75 useConstantArea       no
76
77 #langevinPiston        on
78 #langevinPistonTarget  1.01325 ;#  in bar -> 1 atm
79 #langevinPistonPeriod  200.0
80 #langevinPistonDecay   50.0
81 #langevinPistonTemp    $temperature
82
83 # Output
84 outputName          $outputname
85
86 restartfreq         500     ;# 500steps = every 1ps
87 dcdfreq             100
88 xstFreq             100
89 outputEnergies      100
90 outputPressure      100
91
92 ###################################################################
```

```
93  ## EXTRA PARAMETERS                                              ##
94  ###################################################################
95
96
97  ###################################################################
98  ## EXECUTION SCRIPT                                               ##
99  ###################################################################
100
101 # Minimization
102 #minimize            100
103 #reinitvels          $temperature
104
105 run 20000 ;
```